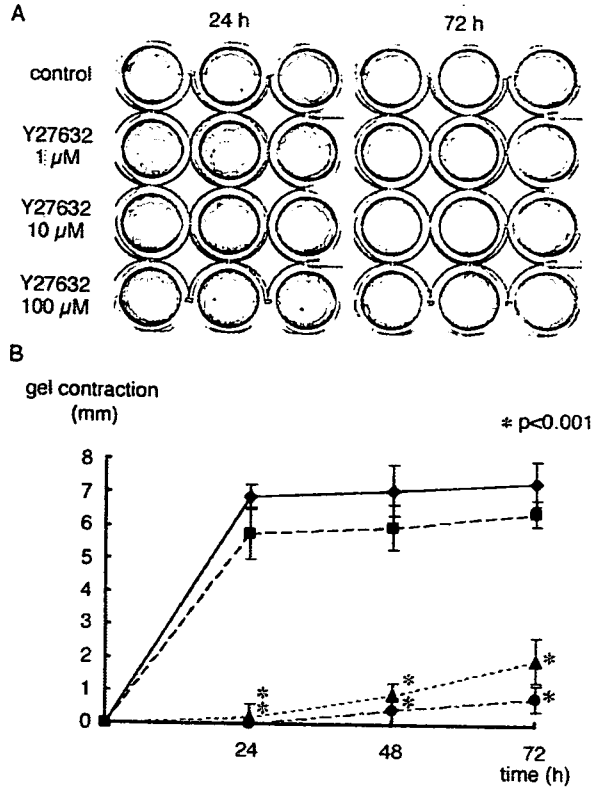

Fig. 5. Effect of Y-27632 on collagen gel contraction by human TM cells. (A) Collagen gels were incubated without (control) or with Y-27632 (1, 10 or 100 μM) for 24 or 72 hr. (B) The changes in diameter of collagen gels in the absence (◆, control) or presence of Y-27632 at 1 (■), 10 (▲) or 100 (●) μM were measured. Data shown as mean ± S.D. ($n=3$) were analysed by Student's t-tests. *$p<0.001$ versus control.

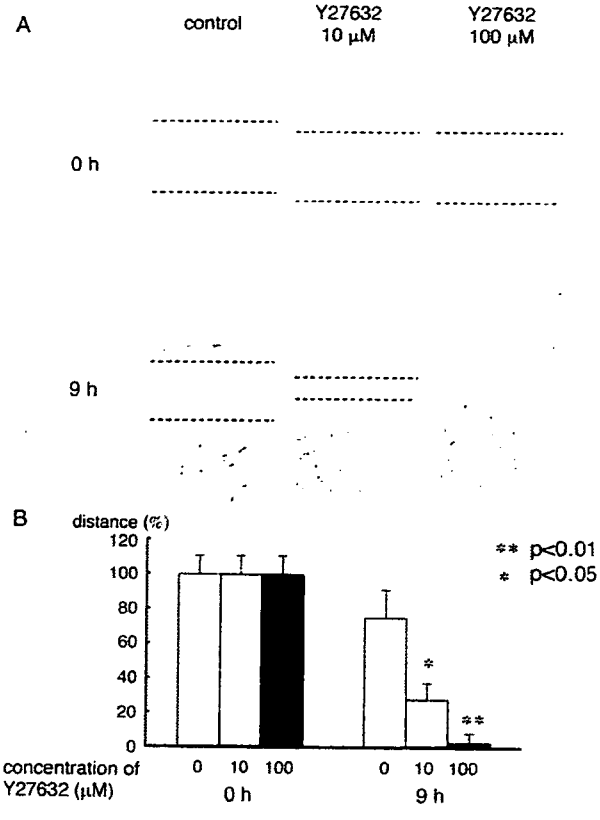

Fig. 6. Effect of Y-27632 on wound healing (motility) activities of human TM cells. (A) The cells grown to confluence were scraped with a yellow pipet tip to create a cell-free line. The medium was replaced with fresh medium without (control) or with 10 or 100 μM Y-27632. After 9 hr, migration of cells into the scraped area was photographed. The edges of migrated cells were indicated as dot lines. (B) The distances between the edges of migrated cells were measured, set at 100% before treatment, and shown as mean ± S.D. ($n=3$). Data were analysed by Student's t-test.

phosphorylated LIM kinase 2 and phosphorylated cofilin (Fig. 7). However, The level of phosphorylated LIM kinase 1 and total cofilin remained unaffected. The observed changes in the phosphorylated forms of LIM kinase 2 and cofilin were reversible after a 2-hr recovery period.

4. Discussion

The present study demonstrates that a specific inhibitor of the ROCK/ROK family of protein kinases, Y-27632, induces profound changes in various behaviours of cultured human TM cells. Exposure to Y-27632 results in cell retraction and rounding of cell bodies with protrusions. Despite these changes, Y-27632 is found not to be toxic. It does not induce cell death nor inhibit proliferation in TM cells.

Our results reveal that TM cellular adhesiveness to the ECM is enhanced by Y-27632. This finding is somewhat unexpected, since in our previous study (Honjo et al., 2001) a decreased focal adhesion formation and loss of actin stress fibres in TM cells were noted after treatment of this inhibitor. The actin cytoskeleton is known to interact with

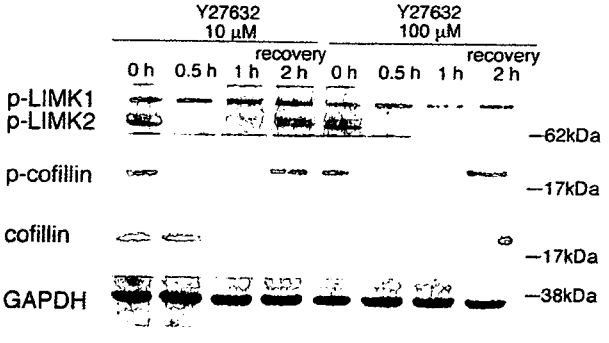

Fig. 7. Effects of Y-27632 on phosphorylation of LIM kinases and that of cofilin in human TM cells. Lysates were collected from cells untreated (control), or treated with 10 or 100 μM Y-27632 for 0.5 or 1 hr. Some dishes, after treatment of 10 or 100 μM Y-27632 for 1 hr, were incubated with fresh culture medium for an additional 2 hr (recovery 2 hr). Immunoblot analysis was performed for phosphorylated LIM kinase 1, phosphorylated LIM kinase 2, and phosphorylated and total cofilin. The levels of these proteins were normalized against that of GAPDH. Experiments were repeated 3 times, yielding similar results.

integrins to regulate cell shape and adhesiveness of cells to the matrix. In experiments using cultured THP-1 monocytes, inhibition of ROCK with Y-27632 did promote integrin adhesion that was accompanied by increases in membrane protrusions and phosphotyrosine signalling (Worthylake and Burridge, 2003). Similarly, in the present study, membrane protrusions were found in human TM cells after Y27632 treatment (data not shown). In addition, phosphotyrosine signalling and focal adhesion-associated molecules were concentrated at periphery of these protrusions by our immunocytochemical analysis (data not shown). The increased cell adhesiveness to ECM might be related to alterations in the cell shape and re-distribution of focal adhesions (and phosphotyrosine signalling) to the cell periphery.

Recent studies have indicated that cytoskeletal drugs including ROCK inhibitor decrease aqueous outflow resistance by destroying or stabilizing a complex of cytoplasmic fibres (Tian et al., 2000). Also, many cytoskeletal drugs have been reported to impair the adhesiveness of cell–cell or cell-matrix. For example, latrunculin-A was reported to be attenuated cell–cell attachments in human TM cells by immunocytochemical analysis (Cai et al., 2000). Protein kinase C inhibitor, which disrupt the actomyosin system, impair TM cell adhesion to ECM by quantitative adhesion assay (Zhou et al., 2000). In our study, protein expression level and distribution of cell–cell associated molecules such as β-catenin and pan-cadherin were almost unchanged after Y27632 treatment. Interestingly, adhesive activity to ECM was increased by the addition of Y27632. Decrease of the number of TM cells, that was observed in glaucomatous eyes, has been thought to be associated with decreased outflow facility and increased IOP (Rohen, 1983; Alvarado et al., 1984; Alvarado et al., 1986). The increased cellular adhesiveness to ECM by Y-27632 may prevent human TM cell decrease from TM tissues in glaucomatous eyes and can distinguish this inhibitor from other cytoskeletal drugs or inhibitors.

Contraction and relaxation of TM tissue are thought to control IOP (Thieme et al., 2000; Nakamura et al., 2002; Nakamura et al., 2003). In a previous study using bovine TM strips, Y27632 reduced TM tissue contraction (Thieme et al., 2000). In the present study, to investigate the direct effect of Y27632 on TM cellular contraction, we used three-dimensional cultures of human TM cells embedded in collagen type I gels. Gel contraction experiments reveal that addition of Y-27632 caused decreased contraction of collagen type I gel by TM cells. This phenomenon suggests reduced cell contractility and/or altered interaction between TM cells and collagen type I. However, as cell adhesion to collagen type I is found increased by addition of Y27632, the gel contraction change is thought to be due to just the TM cell relaxation by Y27632.

Administration of Y-27632, in addition, is shown to enhance motility of TM cells into the wound. This is in accordance with the notion that stabilization of actin stress fibres limits cell movement. Y-27632 also diminished the phosphorylation levels of LIM kinase 2 and cofilin. LIM kinase is the LIM domain-containing serine/threonine/tyrosine kinase composed of closely related LIM kinase 1 and LIM kinase 2 (Okano et al., 1995). They are known to be targets downstream of signalling by Rho GTPases. ROCK, specifically, has been shown to activate LIM kinase 2, but not LIM kinase 1 (Sumi et al., 2001). ROCK phosphorylates and activates LIM kinase 2, which phosphorylates and inactivates cofilin to suppress its actin-depolymerization and actin-severing activity, facilitating stress fibre formation (Bamburg, 1999). Consistent with this model, current experiments indicate that ROCK inhibitor Y-27632 reduces the levels of phosphorylated LIM kinase 2 and cofilin, not LIM kinase 1. The resulting dephosphorylated or active cofilin may in turn in TM cells promote actin depolymerization, formation of cell protrusions, and cell motility. These results suggest that the action of Y-27632 is, at least in part, mediated through the ROCK/LIM kinase 2/cofilin pathway. In previous reports, glucocorticoid, known to decrease aqueous outflow and cause secondary glaucoma, inhibits migration activities of TM cells (Clark et al., 1994). Furthermore, myocilin, known as a gene linked to both juvenile and adult-onset open angle glaucoma, also reduces migration activities of TM cells (Wentz-Hunter et al., 2004). In contrast, interestingly, our study revealed that Y-27632, an IOP lowering drug, accelerated migration activities of TM cells. Taken together, inhibition of migration activities might be associated with decreased aqueous outflow. However, further studies are required to reveal the association of migration activities and outflow facility.

In summary, the present study shows that Y-27632, a selective ROCK inhibitor, alters cellular behaviours of TM cells. It induces a reversible change in cell shape, increases cell adhesion, inhibits gel contraction, and accelerates cell migration. The IOP-lowering effect of Y-27632 observed in animal and perfusion organ culture studies (Honjo et al., 2001; Rao et al., 2001) is thus concluded to be related to the induced changes of TM cellular activities. Also, outflow facility was increased with gene transfer of dominant negative Rho A (Vittitow et al., 2002) or dominant negative binding domain of Rho-kinase (Rao et al., 2005) in anterior segments. The current data further specify that contractility in TM and/or Schlemm's canal cells may be a major factor in the physiology and regulation of the aqueous outflow, and that Rho/ROCK signal transduction is a key mediator of the cell contractility or relaxation. So far there have been accumulating data alluding to the usefulness of ROCK inhibitors as promising drugs in modulating the contractility of cells and lowering the IOP. The lack of toxicity of Y-27632, as demonstrated herein, offers an extra advantage in developing this inhibitor to be a therapeutic means for treatment of glaucoma.

Acknowledgements

This study was supported in part by a Grant-in-Aid for Scientific Research from the Ministry of Education, Science, Sports and Culture, Japan from the Ministry of Health and Welfare, Japan, and grants EY 05628 (BYJTY) and EY 01792 (core) from the National Eye Institute, Bethesda, MD, USA. The authors thank Professor Shuh Narumiya, Department of Pharmacology Kyoto University Faculty of Medicine for his kind advice.

References

Alvarado, J., Murphy, C., Polansky, J., Juster, R., 1981. Age-related changes in trabecular meshwork cellularity. Invest. Ophthalmol. Vis. Sci. 21, 714–727.

Alvarado, J., Murphy, C., Juster, R., 1984. Trabecular meshwork cellularity in primary open-angle glaucoma and nonglaucomatous normals. Ophthalmology 91, 564–579.

Alvarado, J.A., Yun, A.J., Murphy, C.G., 1986. Juxtacanalicular tissue in primary open angle glaucoma and in nonglaucomatous normals. Arch. Ophthalmol. 104, 1517–1528.

Bamburg, J.R., 1999. Proteins of the ADF/cofilin family: essential regulators of actin dynamics. Annu. Rev. Cell Dev. Biol. 15, 185–230.

Bill, A., Phillips, C.I., 1971. Uveoscleral drainage of aqueous humor in human eyes. Exp. Eye Res. 12, 275–281.

Cai, S., Liu, X., Glasser, A., Volberg, T., Filla, M., Geiger, B., Polansky, J.R., Kaufman, P.L., 2000. Effect of latrunculin-A on morphology and actin-associated adhesions of cultured human trabecular meshwork cells. Mol. Vis. 6, 32–43.

Choi, J., Miller, A.M., Nolan, M.J., Yue, B.Y.J.T., Thoz, S.T., Clark, A.F., Agarwal, N., Knepper, P.A., 2005. Soluble CD44 is cytotoxic to trabecular meshwork and retinal ganglion cells in vitro. Invest. Ophthalmol. Vis. Sci. 46, 214–222.

Clark, A.F., Wilson, K., McCartney, M.D., Miggans, S.T., Kunkle, M., Howe, W., 1994. Glucocorticoid-induced formation of cross-linked actin networks in cltured human trabecular meshwork cells. Invest. Ophthalmol. Vis. Sci. 35, 281–294.

Epstein, D.L., Freddo, T.F., Bassett-Chu, S., Chung, M., Karageuzian, L., 1987. Influence of ethacrynic acid on outflow facility in the monkey and calf eye. Invest. Ophthalmol. Vis. Sci. 28, 2067–2075.

Epstein, D.L., Rowlette, L.L., Roberts, B.C., 1999. Acto-myosin drug effects and aqueous outflow function. Invest. Ophthalmol. Vis. Sci. 40, 74–81.

Honjo, M., Tanihara, H., Inatani, M., Kido, N., Sawamura, T., Yue, B.Y.J.T., Narumiya, S., Honda, Y., 2001. Effects of Rho-associated protein kinase inhibitor Y-27632 on intraocular pressure and outflow facility. Invest. Ophthalmol. Vis. Sci. 42, 137–144.

Ishizaki, T., Maekawa, M., Fujisawa, K., Okawa, K., Iwamatsu, A., Fujita, A., Watanabe, N., Saito, Y., Kakizuka, A., Morii, N., Narumiya, S., 1996. The small GTP-binding protein Rho binds to and activates a 160 kDa Ser/Thr protein kinase homologous to myotonic dystrophy kinase. EMBO J. 15, 1885–1893.

Jain, P.T., Pento, J.T., Graves, D.C., 1992. Cell-growth quantitation methods for the evaluation of antiestrogens in human breast cancer cells in culture. J. Pharmacol. Toxicol. Methods 27, 203–207.

Jocson, V.L., Sears, M.L., 1971. Experimental aqueous perfusion in enucleated human eyes. Results after obstruction of Schlemm's canal. Arch. Ophthalmol. 86, 65–71.

Kaibuchi, K., Kuroda, S., Amano, M., 1999. Regulation of the cytoskeleton and cell adhesion by the Rho family GTPases in mammalian cells. Annu. Rev. Biochem. 68, 459–486.

Kaufman, P.L., Barany, E.H., 1977. Cytochalasin B reversibly increases outflow facility in the eye of the cynomolgus monkey. Invest. Ophthalmol. Vis. Sci. 16, 47–53.

Kaufman, P.L., Erickson, K.A., 1982. Cytochalasin B and D dose-outflow facility response relationships in the cynomolgus monkey. Invest. Ophthalmol. Vis. Sci. 23, 646–650.

Khurana, R.N., Deng, P.F., Epstein, D.L., Rao, P.V., 2003. The role of protein kinase C in modulation of aqueous humor outflow facility. Exp. Eye Res. 76, 39–47.

Knepper, P.A., Goossens, W., Hvizd, M., Palmberg, P.F., 1996. Glycosaminoglycans of the human trabecular meshwork in primary open-angle glaucoma. Invest. Ophthalmol. Vis. Sci. 37, 1360–1367.

Leung, T., Manser, E., Tan, L., Lim, L., 1995. A novel serine/threonine kinase binding the Ras-related RhoA GTPase which translocates the kinase to peripheral membranes. J. Biol. Chem. 270, 29051–29054.

Lutjen-Drecoll, E., Gabelt, B.T., Tian, B., Kaufman, P.L., 2001. Outflow of aqueous humor. J. Glaucoma. 10, S42–S44.

Matsui, T., Amano, M., Yamamoto, T., Chihara, K., Nakafuku, M., Ito, M., Nakano, T., Okawa, K., Iwamatsu, A., Kaibuchi, K., 1996. Rho-associated kinase, a novel serine/threonine kinase, as a putative target for small GTP binding protein Rho. EMBO J. 15, 2208–2216.

McMenamin, P.G., Lee, W.R., Aitken, D.A., 1986. Age-related changes in the human outflow apparatus. Ophthalmology 93, 194–209.

Miyazaki, M., Segawa, K., Urakawa, Y., 1987. Age-related changes in the trabecular meshwork of the normal human eye. Jpn. J. Ophthalmol. 31, 558–569.

Nakagawa, O., Fujisawa, K., Ishizaki, T., Saito, Y., Nakao, K., Narumiya, S., 1996. ROCK-I and ROCK-II, two isoforms of Rho-associated coiled-coil forming protein serine/threonine kinase in mice. FEBS Lett. 39, 189–193.

Nakamura, Y., Hirano, S., Suzuki, K., Seki, K., Sagara, T., Nishida, T., 2002. Signaling mechanism of TGF-β1-induced collagen contraction mediated by bovine trabecular meshwork cells. Invest. Ophthalmol. Vis. Sci. 43, 3465–3472.

Nakamura, Y., Sagara, T., Seki, K., Hirano, S., Nishida, T., 2003. Permissive effect of fibronectin on collagen gel contraction mediated by bovine trabecular meshwork cells. Invest. Ophthalmol. Vis. Sci. 44, 4331–4336.

Nobes, C.D., Hall, A., 1995. Rho, Rac and cdc42 GTPases: regulators of actin structures, cell adhesion and motility. Biochem. Soc. Trans. 23, 456–459.

Okano, I., Hiraoka, J., Otera, H., Nunoue, K., Ohashi, K., Iwashita, S., Hirai, M., Mizuno, K., 1995. Identification and characterization of a novel family of serine/threonine kinases containing two N-terminal LIM motifs. J. Biol. Chem. 270, 31321–31330.

Rao, P.V., Deng, P.F., Kumar, J., 2001. Epstein DL. Modulation of aqueous humor outflow facility by the Rho kinase-specific inhibitor Y-27632. Invest. Ophthalmol. Vis. Sci. 42, 1029–1037.

Rao, P.V., Deng, P., Maddala, R., Epstein, D.L., Li, C.Y., Shimokawa, H., 2005. Expression of dominant negative Rho-binding domain of Rho-kinase in organ cultured human eye anterior segments increases aqueous humor outflow. Mol Vis. 11, 288–297.

Riento, K., Ridley, A.J., 2003. ROCKs: multifunctional kinases in cell behavior. Nat. Rev. Mol. Cell Biol. 4, 446–456.

Rohen, J.W., 1983. Why is intraocular pressure elevated in chronic simple glaucoma? Anatomical considerations. Ophthalmology 90, 758–765.

Sawaguchi, S., Yue, B.Y.J.T., Chang, I.L., Wong, F., Higginbotham, E.J., 1992. Ascorbic acid modulates collagen type I gene expression by cells from an eye tissue-trabecular meshwork. Cell Mol. Biol. 38, 587–604.

Sumi, T., Matsumoto, K., Nakamura, T., 2001. Specific activation of LIM kinase 2 via phosphorylation of threonine 505 by ROCK, a Rho-dependent protein kinase. J. Biol. Chem. 276, 670–676.

Takai, Y., Sasaki, T., Tanaka, K., Nakanishi, H., 1995. Rho as a regulator of the cytoskeleton. Trends Biochem. Sci. 20, 227–231.

Thieme, H., Nuskovski, M., Nass, J.U., Pleyer, U., Strauss, O., Wiederholt, M., 2000. Mediation of calcium-Independent contraction in trabecular meshwork through protein kinase C and Rho-A. Invest. Ophthalmol. Vis. Sci. 41, 4240–4246.

Tian, B., Kaufman, P.L., Volberg, T., Gabelt, B.T., Geiger, B., 1998. H-7 disrupts the actin cytoskeleton and increases outflow facility. Arch. Ophthalmol. 116, 633–643.

Tian, B., Geiger, B., Epstein, D.L., Kaufman, P.L., 2000. Cytoskeletal involvement in the regulation of aqueous humor outflow. Invest. Ophthalmol. Vis. Sci. 41, 619–623.

Uehata, M., Ishizaki, T., Satoh, H., Ono, T., Kawahara, T., Morishita, T., Tamalawa, H., Yamagami, K., Inui, J., Maekawa, M., Narumiya, S., 1997. Calcium sensitization of smooth muscle mediated by a Rho-associated protein kinase in hypertension. Nature 389, 990–994.

Vittitow, J.L., Garg, R., Rowlette, L.L., Epstein, D.L., O'Brien, E.T., Borras, T., 2002. Gene transfer of dominant-negative RhoA increases outflow facility in perfused human anterior segment cultures. Mol Vis. 8, 32–44.

Wentz-Hunter, K., Kubota, R., Shen, X., Yue, B.Y.J.T., 2004. Extracellular myocilin affects activity of human trabecular meshwork cells. J. Cell Physiol. 200, 45–52.

Worthylake, R.A., Burridge, K., 2003. RhoA and ROCK promote migration by limiting membrane protrusions. J. Biol. Chem. 278, 13578–13584.

Yue, B.Y.J.T., Higginbotham, E.J., Chang, I.L., 1990. Ascorbic acid modulates the production of fibronectin and laminin by cells from an eye tissue-trabecular meshwork. Exp. Cell Res. 187, 65–68.

Zhou, L., Zhang, S.R., Yue, B.Y., 1996. Adhesion of human trabecular meshwork cells to extracellular matrix proteins. Roles and distribution of integrin receptors. Invest. Ophthalmol. Vis. Sci. 37, 104–113.

Zhou, L., Cheng, E.L., Rege, P., Yue, B.Y.J.T., 2000. Signal transduction mediated by adhesion of human trabecular meshwork cells to extracellular matrix. Exp. Eye Res. 70, 457–465.

Journal of Neurochemistry, 2006, 96, 43–52

doi:10.1111/j.1471-4159.2005.03502.x

NMDA-induced retinal injury is mediated by an endoplasmic reticulum stress-related protein, CHOP/GADD153

Maiko Awai,*[,1] Takahisa Koga,*[,†,1] Yasuya Inomata,* Seiichi Oyadomari,† Tomomi Gotoh,† Masataka Mori† and Hidenobu Tanihara*

*Departments of *Ophthalmology and Visual Science and †Molecular Genetics, Kumamoto University Graduate School of Medical Sciences, Kumamoto, Japan*

Abstract

We investigated the role of an endoplasmic reticulum stress-associated protein, CHOP/GADD153, after NMDA-induced mouse retinal damage. After injection of NMDA into the vitreous, TUNEL-positive cells were detected in the retinal ganglion cell layer (GCL) and inner nuclear layer (INL) at 6 h after NMDA injection, and these gradually increased in number up to 24 h. Analysis by real-time RT-PCR revealed that CHOP mRNA was induced by about 3-fold, at 2 h after NMDA injection. Immunoreactivity for the CHOP protein was intense in cells of the GCL following NMDA treatment. Immunoblot analysis showed that NMDA injection increased the expression of CHOP protein in the retina. Compared with wild-type mice, $CHOP^{-/-}$ mice were more resistant to NMDA-induced retinal cell death as determined by TUNEL assay. At 7 days after NMDA treatment, the thickness of the inner plexiform layer and INL were larger in $CHOP^{-/-}$ mice than in wild-type mice. The number of residual cells in the GCL following NMDA treatment was significantly higher in $CHOP^{-/-}$ mice than in wild-type mice. In conclusion, CHOP is induced in mouse retina by NMDA treatment, and $CHOP^{-/-}$ mice are more resistant to NMDA-induced retinal damage, suggesting that CHOP plays an important role in NMDA-induced retinal cell death.

Keywords: C/EBP homologous protein, endoplasmic reticulum, NMDA, retinal ganglion cells.

J. Neurochem. (2006) **96**, 43–52.

Apoptotic cell death is associated with various retinal disorders, including human and experimental retinitis pigmentosa (Reme *et al.* 1998; Farrar *et al.* 2002), retinal ischaemia of animal model (Kuroiwa *et al.* 1998; Rosenbaum *et al.* 1998), and experimental glaucoma (Quigley *et al.* 1995) and human glaucoma (Kerrigan *et al.* 1997; Wax *et al.* 1998). Glutamate, an excitatory amino acid, causes retinal neuronal cell death. The *N*-methyl-D-aspartate (NMDA) receptor, which is one of the glutamate receptors, has been implicated in retinal neuronal cell death (Lam *et al.* 1999a). Administration of NMDA into animal vitreous cavities induced cell death in the ganglion cell layer (GCL) and inner nuclear layer (INL) of the retina (Joo *et al.* 1999). This retinal injury model has been widely used to investigate the mechanism of retinal neuronal cell death and to investigate neuroprotective factors and drugs (Inomata *et al.* 2003a,b).

The endoplasmic reticulum (ER) is an intracellular Ca^{2+} storage compartment in most cells. In the ER, newly synthesized 'secretary' proteins undergo glycosylation, disulfide bond formation, folding and oligomerization. These activities strictly depend on a high Ca^{2+} concentration in the ER (Alberts *et al.* 2002). Exposure of neurons to glutamate activates glutamate receptors and raises cytosolic Ca^{2+} levels.

Received April 21, 2005; revised manuscript received July 19, 2005; accepted August 22, 2005.

Address correspondence and reprint requests to Hidenobu Tanihara MD, Department of Ophthalmology, Kumamoto University School of Medicine, 1-1-1 Honjo, Kumamoto, 860–8556, Japan.
E-mail: tanihara@pearl.ocn.ne.jp

[1]These authors contributed equally to this work.

Abbreviations used: ARVO, Association for Research in Vision and Ophthalmology; ASK, apoptosis signal-regulating kinase; CHOP, C/EBP homologous protein; ECL, enhanced chemiluminescence; ER, endoplasmic reticulum; GADD153, growth arrest and DNA damage-inducible gene 153; GAPDH, glyceraldehyde-3-phosphate dehydrogenase; GCL, ganglion cell layer; HRP, horseradish peroxidase; INL, inner nuclear layer; NIH, National Institutes of Health; PAGE, polyacrylamide gel electrophoresis; PBS, phosphate-buffered saline; PI, propidium iodide; RGCs, retinal ganglion cells; SDS, sodium dodecyl sulfate; TBS, Tris-buffered saline; TSA, tyramide signal amplification; TUNEL, terminal deoxyribonucleotidyl transferase (TdT)-mediated fluroscein-16-dUTP nick-end labelling.

Ca^{2+} first enters the cytosol from the extracellular space through glutamate receptors, and then a large amount of Ca^{2+} is released from the ER to the cytosol (Paschen and Frandsen 2001; Hajnoczky *et al.* 2003). Disturbance of Ca^{2+} homeostasis in the ER leads to its dysfunction. Other conditions such as hypoxia, hypoglycaemia, and mutation of 'secretory' protein genes induce ER dysfunction and ER stress (Kaufman *et al.* 2002; Oyadomari *et al.* 2002a,b; Oyadomari and Mori 2004). When cells experience severe ER stress, the C/EBP homologous protein (CHOP), also known as growth arrest and DNA damage-inducible gene 153 (GADD 153), is induced in certain cell types (Ron and Habener 1992; Barone *et al.* 1994; Oyadomari *et al.* 2002a,b). CHOP is expressed at low levels under physiological conditions and is highly induced in response to ER stress (Ron *et al.* 1992). Induction of CHOP plays a key role in the pathway of ER stress-mediated apoptosis (Kawahara *et al.* 2001; Oyadomari *et al.* 2001; Gotoh *et al.* 2002; Oyadomari *et al.* 2002a,b; Gotoh *et al.* 2004; Oyadomari *et al.* 2004; Tajiri *et al.* 2004; Tsutsumi *et al.* 2004).

In this study, we report that CHOP is induced in cells of the GCL following NMDA treatment and that CHOP-deficient mice are more resistant to NMDA-induced retinal neuronal cell death.

Materials and methods

NMDA-induced retinal injury

All experiments conformed to the ARVO Statement for the Use of Animals in Ophthalmic and Vision Research. $CHOP^{-/-}$ mice (C57 BL/6 background) were provided by Dr Shizuo Akira (Osaka University, Japan). C57 BL/6 and $CHOP^{-/-}$ male mice, 8–12 weeks old, were used in this study. Mice were anaesthetized by intramuscular injection of 0.025 mg of ketamine hydrochloride (Sankyo, Tokyo, Japan) and 0.1 mg of xylazine (Bayer, Leverkusen, Germany). After the pupil was dilated with phenylephrine hydrochloride and tropicamide, injection into the vitreous cavity was performed under a microscope using a 33-gauge needle connected to a microsyringe and inserted toward to the posterior pole carefully, and not inserted too deep to avoid lens damage, approximately 1 mm behind the corneal limbus. NMDA and NMDA antagonst, MK-801 were obtained from Sigma (St Louis, MO, USA). A single dose of 2 mL of sterilized phosphate-buffered saline (PBS) containing NMDA was injected into the vitreous cavity. Some mice were systemically treated with 0.01 mg of MK-801 through a single injection into the peritoneal cavity 1 h before intravitreous NMDA injection. Control mice received either no injection or an injection of 2 mL of PBS into the vitreous cavity.

Real-time reverse transcription-polymerase chain reaction (RT-PCR) of CHOP mRNA

NMDA (5 nmol/2 mL) was injected into the vitreous cavity in C57 BL/6 mice. At 2, 6, 12 and 24 h after NMDA injection, mice were killed. At 2, 6 and 12 h, PBS-injected mice or NMDA-injected mice after pretreatment with MK-801(0.01 mg) were also killed. Eyes were dissected immediately, and total RNA was isolated from mouse retina using the AquaPure RNA isolation kit (Bio-Rad Laboratories, Hercules, CA, USA). To remove genomic DNA, the total RNA preparation was treated with deoxyribonuclease I (Invitrogen, Carlsbad, CA, USA). Assay-on-demand primers and probes systems (Applied Biosystems, Foster City, CA, USA) were used to quantify mRNAs for mouse CHOP Assay ID; Mm 00492097 and glyceraldehydes-3-phosphate dehydrogenase (GAPDH Assay ID; Mm 999999 15). These commercially available primers and probes sets, whose sequences were undocumented and whose PCR products were composed to be about 100 base pairs, were widely used (Staller *et al.* 2003; Tokuhiro *et al.* 2003; Roy *et al.* 2004). These primer sets were designed to span exon–exon junctions to eliminate any influence from the presence of contaminant genomic DNA. Real-time RT-PCR was performed with 10 ng of total RNA on an ABI Prism 7000 Sequence Detection System (Applied Biosystems) using the SuperScript One-Step RT-PCR system (Gibco BRL, Grand Island, NY, USA). Total RNA was reverse transcribed into cDNA using one cycle at 50°C for 30 min and one cycle at 95°C for 10 min cDNA was amplified using 40 cycles at 94°C for 15 s and 60°C for 1 min. Fluorescence changes of SYBR Green, the green fluorescent dye were monitored after each cycle. Melting curve analysis was performed (0.5°C/s increase from 55°C to 95°C with continuous fluorescence readings) at the end of 40 cycles to ensure that specific PCR products were obtained. The threshold cycle of fluorescence units was evaluated to quantify the amount of each mRNA level. Each CHOP mRNA level was normalized by the GAPDH mRNA level, and expressed as a mean ± standard deviation. The adjusted CHOP mRNAs after NMDA treatment were statistically analyzed using the ANOVA test. PCR products after 25 cycles for CHOP gene and 25 cycles for GAPDH gene were run by electrophoresis on a 1.5% agarose gel, to check size of PCR (and reaction specificity) and to confirm quantificative results of real-time RT-PCR.

Immunohistochemical staining

NMDA (5 nmol/2 mL) was injected into the vitreous cavity in C57 BL/6 mice. Mice were killed at 2, 6 and 12 h after NMDA injection. As control experiments, mice were treated with either intravitreous PBS injection or intravitreous NMDA injection after 0.01 mg of MK-801 pretreatment. The eyes were immediately enucleated and fixed with 4% paraformaldehyde in PBS. Specimens were dehydrated and embedded into paraffin. Transverse paraffin sections (3-mm thick), including the optic disc, were soaked in xylene, rehydrated in graded ethanols, and then washed with PBS. Sections were treated with 50 mg/mL trypsin and then washed three times. Each section was incubated for 30 min in PBS containing 2% horse serum and 5% skim milk to block non-specific binding. Monoclonal anti-mouse CHOP antibody (Santa Cruz Biotechnology, Santa Cruz, CA, USA) was used at a dilution of 1 : 200 in PBS containing 5% skim milk. Sections were incubated with this antibody overnight at 4°C and then washed three times in PBS. Sections were then incubated with mouse anti-mouse IgG HRP (horseradish peroxidase) antibody (Amersham, Buckinghamshire, UK) for 1 h at room temperature at a dilution of 1 : 500 in PBS. After washing with PBS three times, sections were amplified using the TSA (tyramide signal amplification) biotin system (PerkinElmer, Boston, MA, USA). They were incubated in the biotinyl tyramide

amplification reagent (Perkin Elmer) for 15 min at room temperature and washed with PBS three times. Following this, all slides were incubated with streptavidin Alexa Fluor 488 conjugate (Molecular Probes, Eugene, OR, USA) at a dilution of 1 : 500 in PBS for 30 min in the dark. After washing with PBS, sections were stained with propidium iodide (PI) for 15 min in the dark to illustrate retinal cell distribution and to clear retinal layers such as GCL, INL and outer nuclear layer. After washing with PBS, the number of CHOP-positive cells (in GCL and INL) and the number of PI stained cells (in GCL) were counted at 1.0–1.5 mm from the optic disc using a confocal microscope FV300 (Olympus, Tokyo, Japan), and expressed in millimetres. The percentage of the number of CHOP positive cells for that of PI stained cells was calculated in GCL of mouse retina. One section of each mouse eye was used for counting.

Immunoblot analysis

NMDA (5 nmol/2 mL) was injected into the vitreous cavity in C57 BL/6 mice. At 6 h after NMDA injection, mice were killed. As control experiments, PBS-injected mice or NMDA-injected mice after pretreatment of MK-801 (0.01 mg) were also killed. The retinal tissue was immediately isolated and lysed with lysis buffer containing 1% Nonidet P-40, 150 mM NaCl, 50 mM Tris-HCl (pH 7.4), 1 mM EDTA, 0.25% sodium deoxycholate, and a protease inhibitor tablet, Complete Mini (Roche Molecular Biochemicals, Mannheim, Germany). Lysates were subjected to sodium dodecyl sulfate – polyacrylamide gel electrophoresis (SDS–PAGE) using a 12% Tris-glycine gel (Invitrogen). Following electrophoresis, proteins were transferred to nitrocellulose membranes. Membranes were blocked for 30 min at room temperature using a blocking solution containing 5% skim milk powder and 0.1% Tween-20 in Tris-buffered saline (TBS; pH 7.4), and then incubated with monoclonal anti-mouse CHOP antibody overnight at 4°C diluted 1 : 100 in TBS or monoclonal anti-mouse β-actin antibody (Sigma) diluted 1 : 50000 in TBS for 60 min at room temperature. Membranes were then washed three times and incubated with mouse anti-mouse IgG HRP antibody (Amersham) for 30 min at room temperature at a dilution of 1 : 4000 in TBS. Membranes were washed three times, treated with an enhanced chemiluminescence (ECL) western blotting detection reagent (Amersham) and then exposed to X-ray film. The density of the signal was quantified using NIH (National Institutes of Health) Image 6.2 software and CHOP expression levels were normalized for β-actin. Results are expressed as a mean ± standard deviation for four independent experiments and analyzed statistically using the ANOVA test. An extract of mouse NIH3T3 cells treated with 1 mM thapsigargin (Sigma) for 6 h was used as positive control.

Terminal deoxyribonucleotidyl transferase (TdT)-mediated fluorescein-16-dUTP nick-end labelling (TUNEL) assay

To compare the number of TUNEL-positive cells in wild-type and $CHOP^{-/-}$ mice, a single dose of 2 mL PBS containing 1, 2, 5 or 10 nmol of NMDA was injected into the vitreous cavity. At 24 h after NMDA injection, mice were killed. Eyes were immediately enucleated and fixed with 4% paraformaldehyde in PBS. After specimens were dehydrated and embedded into paraffin, 5-mm thick transverse sections, including the optic disc, were cut. Sections were soaked in xylene to remove paraffin, rehydrated in graded ethanols, and then washed with PBS. The TUNEL assay was performed using the Apoptosis Detection System, Fluorescein (Promega, Madison, WI, USA) according to the manufacturer's protocol. The sections were stained with PI. The number of TUNEL-positive cells (in GCL and INL) and that of PI stained cells (in GCL) were counted at 1.0–1.5 mm from the optic disc under a confocal microscope FV300, and expressed in millimetres. The percentage of the number of TUNEL-positive cells for that of PI stained cells was calculated in the GCL of mouse retina. One section of each mouse eye was used for counting. Data were analyzed using the Student's *t*-test.

Morphometric analysis

Morphometric analysis was conducted as previously described (Inomata *et al.* 2003a,b). $CHOP^{-/-}$ mice and age-matched C57 BL/6 male mice were used in this analysis. Briefly, at 7 days after 2 nmol NMDA injection, mice were killed and eyes were enucleated. The eyes were immersed in 2.5% glutaraldehyde and 2% paraformaldehyde in PBS overnight at 4°C, followed by dehydration and paraffin embedding. Transverse sections 3 mm in thickness, including the optic disc, were prepared from the mouse eyes. Sections were stained with hematoxylin–eosin and photographed at 1.0 mm from the optic disc. The thickness of the inner plexiform layer, INL, outer plexiform layer, and outer nuclear layer was measured and shown as a mean ± standard deviation. The number of residual cells in the GCL (1.0–1.5 mm from the optic disc) was counted and expressed a mean ± standard deviation (in millimetres). One section of each mouse eye was used for counting. Data were analyzed using the Student's *t*-test.

Results

Real-time RT-PCR analysis using total RNA derived from mouse retina was performed to quantify CHOP mRNA expression following NMDA injection (Fig. 1). At 2 h after NMDA treatment, the relative expression level of CHOP mRNA increased to 316 ± 116% of the basal level ($p = 0.005$; 0 vs. 2 h, $p = 0.010$; 2 vs. 24 h, ANOVA). It then decreased to 220 ± 126, 219 ± 116, and 121 ± 68%, at 6, 12 and 24 h after NMDA injection, respectively. After PBS injection, the relative expression level of CHOP mRNA significantly increased to 179 ± 74% of the basal level ($p = 0.010$; 0 vs. 2 h, $p = 0.007$; 2 vs. 6 h, $p = 0.004$; 2 vs. 12 h, ANOVA). After then it was decreased to almost basal level. Similarly, it was significantly increased at 2 h after NMDA treatment in the eyes with pretreatment with MK-801 ($p = 0.007$; 0 vs. 2 h, $p = 0.002$; 2 vs. 6 h, $p = 0.0002$; 2 vs. 12 h, ANOVA). After then, it was decreased to almost basal level. By TUNEL staining assay, TUNEL-positive cells appeared in GCL and INL after 6 h, and then increased up to 24 h after NMDA treatment. However, TUNEL-positive cells were undetectable at any time points (2, 6, 12, 24 h) either in the eyes injected with PBS or in the eyes injected with NMDA after systemic MK-801 pretreatment (data not shown).

In our immunohistochemical analysis, immunoreactivity for CHOP was not conspicuous in the mouse retina under normal conditions (Fig. 2). At 2 h after NMDA injection,

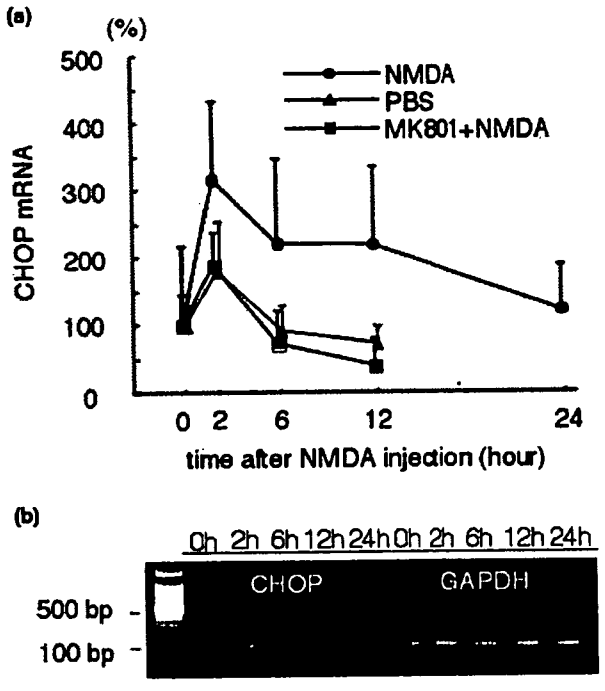

Fig. 1 Expression of CHOP mRNA in mouse retina following NMDA treatment. (a) Real-time RT-PCR analysis of CHOP mRNA was performed after intravitreous NMDA (black) or PBS (green) injection. Some mice were systemically pretreated with MK-801 before intravitreous NMDA injection (red). CHOP mRNA was standardized with GAPDH mRNA. CHOP mRNA was set at 100% in control and expressed as a mean ± standard deviation (n = 5–8). Data were analyzed using the ANOVA test. Asterisks indicate statistically significant differences. (b) RT-PCR experiment of CHOP mRNA and GAPDH mRNA after NMDA injection is shown.

CHOP immunoreactivity was found in cells present in the GCL, and the mean number of CHOP-positive cells in the GCL increased to 6.1 ± 5.6 cells/mm (p = 0.037; 0 vs. 2 h, ANOVA). At 6 h after NMDA treatment, CHOP-positive cells significantly increased to 30.9 ± 1.8 cells/mm in the GCL (p < 0.0001; 0 vs. 6 h, 2 vs. 6 h, 6 vs. 12 h, ANOVA). At 12 h after NMDA treatment, the number of CHOP-positive cells decreased to near basal levels (0.6 ± 1.1 cells/mm). In contrast, no CHOP-positive cells were found in control experiments at any time points either with intravitreous injection of PBS or with intravitreous injection of NMDA after systemic MK-801 pretreatment. Additionally, an immunoblot assay was performed to evaluate the relative expression level of CHOP protein (Fig. 3). Under normal conditions, CHOP protein was faintly detected in immunoblot experiments of mouse retinal samples. In both PBS-injected eyes and NMDA-injected eyes after pretreatment with MK-801, the expression level for CHOP protein was almost the same level as that in the untreated eye. After NMDA injection, the relative expression level of CHOP increased to 178 ± 21% of basal levels (p = 0.001; no treatment vs. NMDA, p = 0.0005; PBS vs. NMDA, ANOVA).

The TUNEL assay was performed in the mouse retina of the two strains 24 h after NMDA treatment (Fig. 4). In control experiments using PBS injection, no TUNEL-positive cells were found in C57 BL/6 and CHOP$^{-/-}$ mice. Furthermore, following intravitreous injection of 1 nmol NMDA, only a small number of TUNEL-positive cells were found in the retina of C57 BL/6 and CHOP$^{-/-}$ mice. However, following injection of 2 nmol NMDA, the mean number of TUNEL-positive cells in the GCL of CHOP$^{-/-}$ mice (6.8 ± 3.8 cells/mm) were significantly lower than that of C57 BL/6 mice (18.8 ± 7.4 cells/mm, p = 0.025, Student's t-test). Similarly, the percentage of CHOP positive cells for TUNEL-stained cells in the GCL of CHOP$^{-/-}$ mice (6.4 ± 3.7%) was significantly lower than that of C57 BL/6 mice (16.8 ± 4.9%, p = 0.001, Student's t-test). Furthermore, the number of TUNEL-positive cells in the INL of CHOP$^{-/-}$ mice (5.0 ± 3.7 cells/mm) was significantly lower than the number in C57 BL/6 mice (19.8 ± 4.6 cells/mm, p = 0.001, Student's t-test). After injection of 5 nmol NMDA, the mean number of TUNEL-positive cells in the GCL of CHOP$^{-/-}$ mice (15.3 ± 13.1 cells/mm) was significantly lower than the number in C57 BL/6 mice (36.3 ± 7.5 cells/mm, p = 0.036, Student's t-test). Similarly, the percentage of CHOP-positive cells to TUNEL-stained cells in the GCL of CHOP$^{-/-}$ mice (18.1 ± 14.9%) was significantly lower than that of C57 BL/6 mice (48.9 ± 6.3%, p = 0.001, Student's t-test). However, there was no significant difference in the number of TUNEL-positive cells in the INL of CHOP$^{-/-}$ (37.3 ± 19.3 cells/mm) and C57 BL/6 (44.3 ± 8.2 cells/mm) mice. Additionally, in experiments using a large amount of NMDA (10 nmol), no statistically significant difference was found in either the GCL or INL of these two strains.

Morphological changes were then measured in experiments employing two strains (C57 BL/6 and CHOP$^{-/-}$) following intravitreal injection of 2 nmol NMDA (Fig. 5). In both C57 BL/6 and CHOP$^{-/-}$ mice, the thickness of the inner plexiform layer and INL decreased significantly following NMDA injection. The mean thickness of the IPL in CHOP$^{-/-}$ and in C57 BL/6 mice was 20.3 ± 5.4 and 14.7 ± 4.2 mm, respectively, showing a significant difference (p = 0.018, Student's t-test). Similarly, the mean thickness of the INL in CHOP$^{-/-}$ and in C57 BL/6 mice was 22.7 ± 4.8 and 18.5 ± 3.5 mm, respectively (p = 0.040, Student's t-test). Additionally, in experiments with NMDA treatment, the number of cells in the GCL of CHOP$^{-/-}$ mice was 34.8 ± 11.4 cells/mm, which was higher than that in C57 BL/6 mice (24.1 ± 7.7 cells/mm, p = 0.026, Student's t-test). In contrast, in the outer retinal layers such as the outer plexiform and outer nuclear layers, no difference was observed. Furthermore, in control experiments using intravitreous PBS injection, there was no significant difference in the thickness of any retinal layers of C57 BL/6 and CHOP$^{-/-}$ mice.

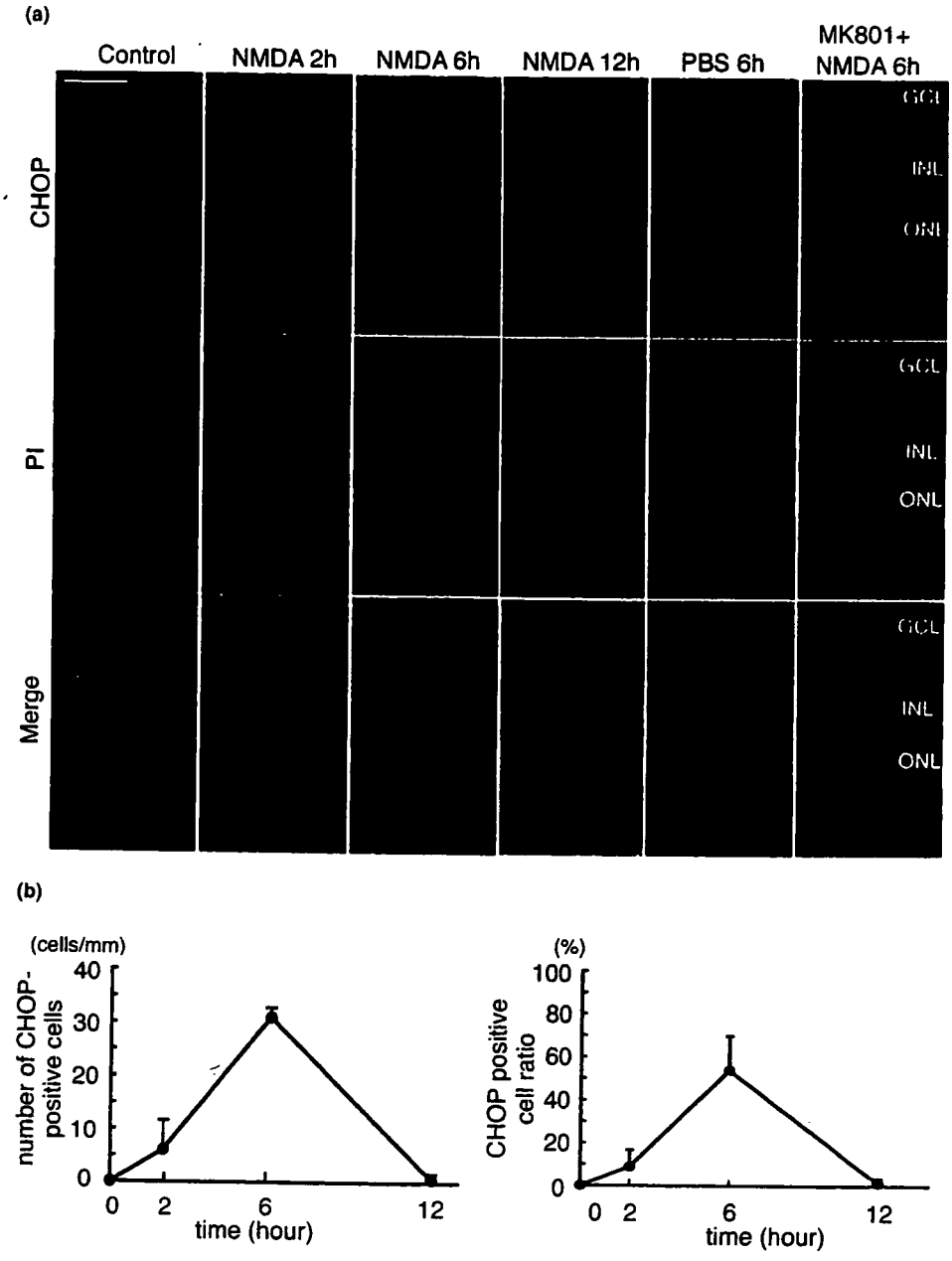

Fig. 2 Immunohistochemical analysis for CHOP protein in mouse retina following NMDA treatment. (a) Immunohistochemical analysis was performed in the eyes with NMDA injection, PBS injection, or NMDA injection after systemic MK-801 treatment. Propidium iodide (PI) staining was also performed. GCL, ganglion cell layer; INL, inner nuclear layer; ONL, outer nuclear layer. Scale bar: 50 mm. (b) The number of CHOP-positive cells was counted and shown as a mean ± standard deviation ($n = 3$). The ratio of CHOP-positive cells/PI stained cells was also shown.

Discussion

In a number of visual-threatening ocular diseases such as ischaemic retinal disease and glaucoma, glutamate toxicity has been regarded as one of the major mechanisms related to retinal neuronal cell death (Kuroiwa *et al.* 1998; Dkhissi *et al.* 1999; Lam *et al.* 1999a,b). This hypothesis is supported by the fact that glutamate receptor antagonists show a neuroprotective effect against some forms of retinal injury and ocular hypertension (glaucoma) in animal experiments (Rosner *et al.* 1997; Chaudhary *et al.* 1998; Sun *et al.* 2001). Recently, notions pertaining to the involvement of ER stress

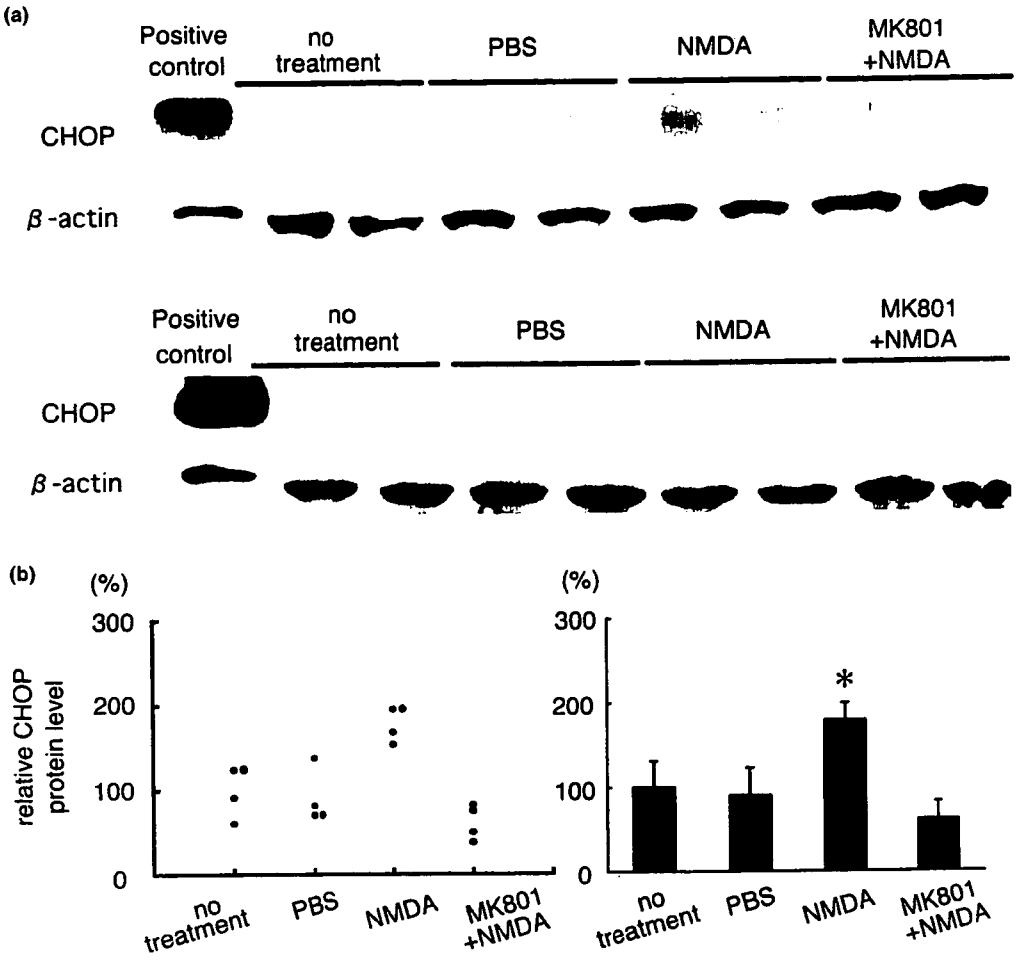

Fig. 3 Immunoblot analysis of CHOP protein following NMDA injection. (a) The homogenates from the retina with no injection, PBS injection, NMDA injection, or NMDA injection after MK-801 pretreatment were subjected to immunoblot analysis. The homogenate from NIH3T3 cells treated with 1 mM thapsigargin was used as a positive control. (b) The amount of CHOP protein was quantified by densitometric analysis and standardized for β-actin. The average of CHOP protein in the retina with no treatment was set at 100%. Data ($n = 4$) were indicated as dot in the left graph. Data are shown as a mean ± standard deviation in the right graph. Data were analyzed using the ANOVA test. Asterisks indicate statistically significant differences.

in neuronal damage have received much attention by investigators. The molecular mechanisms involved have been shown to play an important role in neurodegenerative disorders such as Alzheimer's disease (Mattson and Chan 2003; Katayama *et al.* 2004; Pereira *et al.* 2004), Parkinson's disease (Imai *et al.* 2000; Chen *et al.* 2004), polyglutamine diseases (Kouroku *et al.* 2002; Nishitoh *et al.* 2002; Takeda *et al.* 2002), and brain ischaemia (DeGracia and Montie 2004; Kitano *et al.* 2004). To date, however, there has been no investigation concerning the involvement of ER stress in the pathogenesis of retinal injury (or glaucoma). Among the ER stress-related molecules, CHOP is known to be highly induced in response to ER stress and is implicated to play a role in apoptosis (Ron *et al.* 1992). Induction of this molecule is thought to play an important role in the pathway of ER stress-mediated apoptosis (Kawahara *et al.* 2001; Oyadomari *et al.* 2001; Gotoh *et al.* 2002; Oyadomari *et al.* 2002a,b; Gotoh *et al.* 2004; Oyadomari *et al.* 2004; Tajiri *et al.* 2004; Tsutsumi *et al.* 2004). A previous report of gene-array analysis on NMDA-induced retinal injury showed an up-regulation of some molecules, including a 3.7-fold increase in CHOP (Laabich *et al.* 2001). This exhaustive assay, using microarray, already predicted the importance of the CHOP gene in NMDA retinal injury. In the present study, we clearly showed the important role of the CHOP gene in neuronal cell death in NMDA-induced retinal damage.

Our results from a series of experiments showed that CHOP is up-regulated in eyes with NMDA-induced retinal injury. Real-time RT-PCR experiments showed that the relative level of CHOP mRNA expression peaked at 2 h after

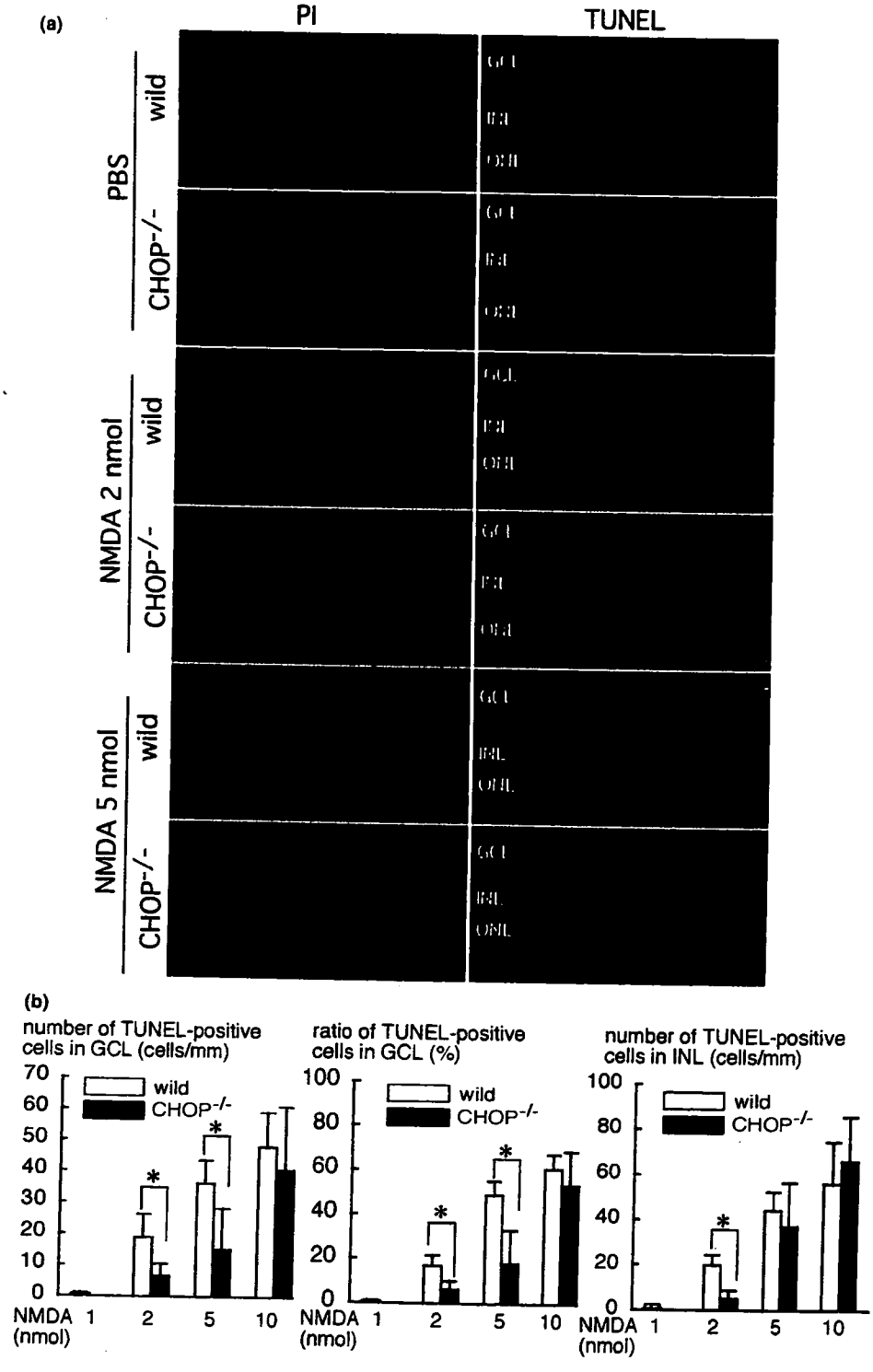

Fig. 4 (a) Terminal deoxyribonucleotidyl transferase (TdT)- mediated fluorescein-16-dUTP nick-end labelling (TUNEL) staining of wild-type and CHOP$^{-/-}$ mouse retina at 24 h after NMDA treatment. Propidium iodide (PI) staining was also performed. Scale bar: 50 mm. GCL, ganglion cell layer; INL, inner nuclear layer; ONL, outer nuclear layer. (b) The number of TUNEL-positive cells in GCL and that in INL were counted and expressed as a mean ± standard deviation ($n = 4$–6). The ratio of TUNEL-positive cells/PI stained cells was calculated and shown. Data were analyzed using the Student's *t*-test.

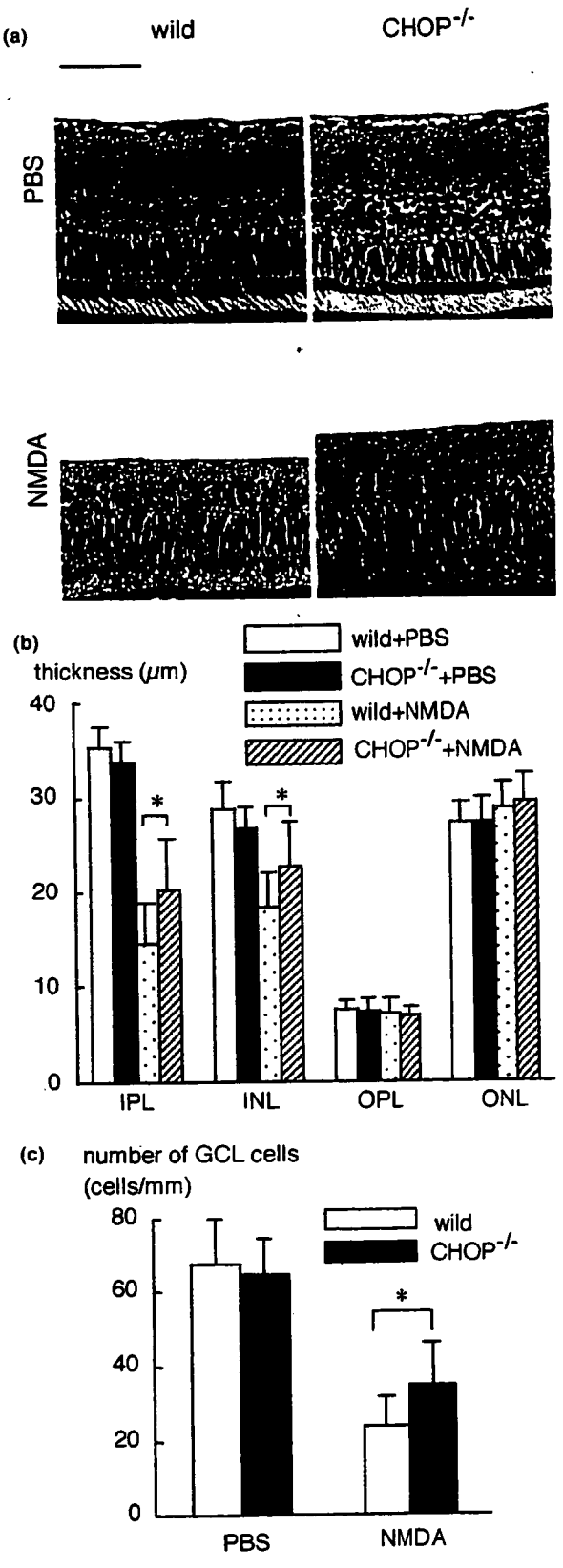

Fig. 5 Morphological analysis of wild-type and CHOP$^{-/-}$ mouse retina at 7 days after 2 nmol NMDA treatment. (a) Paraffin sections stained with hematoxylin-eosin. GCL, ganglion cell layer; IPL, inner plexiform layer; INL, inner nuclear layer; OPL, outer plexiform layer; ONL, outer nuclear layer; PR, photoreceptor. (b) The thickness of retinal layers such as IPL, INL, OPL and ONL was measured and shown as a mean ± standard deviation (n = 10). Data were analyzed using the Student's t-test. Scale bar: 50 mm. (c) The number of residual cells in the ganglion cell layer was counted and shown as a mean ± standard deviation. Data were analyzed using the Student's t-test.

NMDA injection. Given that CHOP immunoreactivity in retinal sections of the GCL peaked at 6 h after NMDA treatment, up-regulated expression of the CHOP protein can be expected to follow the increased expression of CHOP mRNA. However, in either of the eyes with PBS injection or those with NMDA injection after MK-801 treatment, mRNA for CHOP was induced in our real-time RT-PCR study, but CHOP protein induction was not observed in our immunohistochemical and immunoblot studies. It seemed that inductions of CHOP protein in these control eyes were under the detection limits of our assays. All these results may imply a contribution of CHOP to the onset and progression of apoptotic cell death in retinal tissue caused by NMDA, as TUNEL-positive cells appeared after 6 h, and then increased during the following 24 h after NMDA treatment.

It was somewhat surprising that CHOP protein was induced strongly in retinal cells of the GCL but little expressed in retinal cells of INL, although TUNEL-positive cells were observed in both the GCL and INL. A number of retinal ganglion cells are located in the GCL, and apoptosis of these cells plays a key role in the pathogenesis of glaucoma, a major cause of blindness (Quigley *et al.* 1995; Rosenbaum *et al.* 1998). It was known that susceptibility for ER stress differs markedly from cell to cell, and organ to organ. The pancreatic β-cell, having abundant ER in the cytoplasm and synthesizing insulin vigorously, is one of the most susceptible cells for ER stress (Oyadomari *et al.* 2001). Ultrastructural observations have demonstrated that the cytoplasm of retinal ganglion cells contains abundant ER, suggesting active synthesis of 'secretary' proteins (Sigelman *et al.* 1982). Retinal ganglion cells might be more susceptible to ER stress than other retinal cells in INL. Our observation of increased expression of CHOP protein in retinal cells of GCL may be associated with these cell characteristics of retinal ganglion cells.

ER functions as an intracellular calcium store and plays an important role in Ca^{2+} homeostasis by pumping Ca^{2+} via the ER rumen (Paschen 2003). NMDA caused Ca^{2+} influx from the ER to cytosol, and resulted in ER Ca^{2+} depletion and ER stress (Paschen *et al.* 2001). ER stress followed by Ca^{2+} depletion induces the CHOP gene (Oyadomari *et al.* 2004). In our report, overexpression of calreticulin, a major binding protein in ER, increases ER Ca^{2+} stores and protects against

nitric oxide-induced (CHOP-mediated) apoptosis (Oyadomari *et al.* 2001). As mentioned above, it was thought that NMDA depletes ER Ca^{2+} stores, leads ER dysfunction and CHOP protein induction in retinal cells in the GCL. However, the precise apoptosis cascade downstream of CHOP is not well known. It was reported that overexpression of Bcl-2 blocked CHOP-induced apoptosis (Matsumoto *et al.* 1996) and overexpression of CHOP leads to a decrease in Bcl-2 protein (McCullough *et al.* 2001). We recently found that CHOP-induced apoptosis in RAW 264.7 macrophages is mediated by translocation of Bax from the cytosol to the mitochondria (Gotoh *et al.* 2004). Further study is required to reveal in detail the cascade of CHOP downstream.

Morphological abnormality was not seen in adult ocular tissues of $CHOP^{-/-}$ mice. $CHOP^{-/-}$ mice were reported to display normal development and fertility (Zinszner *et al.* 1998; Oyadomari *et al.* 2001). Similarly, normal development and fertility was reported in other ER stress-related gene knockout mice, such as caspase $12^{-/-}$ mice and ASK1 (apoptosis signal-regulating kinase)$^{-/-}$ mice (Nakagawa *et al.* 2000; Tobiume *et al.* 2001). Therefore, knockout of the CHOP gene would probably not cause serious developmental abnormalities, because this gene might not have such an important role in ocular development. However, our present study demonstrated that $CHOP^{-/-}$ mice are more resistant to retinal injury when the injury was caused with low doses (2–5 nmol) of NMDA. Our results showed that the neuroprotective effects in CHOP-deficient mice against NMDA-induced retinal injury were limited. We speculate that other CHOP-independent apoptosis cascades, such as oxidative stress and DNA damage, might cause neuronal cell death in $CHOP^{-/-}$ mice. In the experiments using pancreatic b-cells, low doses of nitric oxide depleted ER Ca^{2+}, led to ER dysfunction, induced CHOP protein, and resulted in apoptosis. As the dose of nitric oxide was increased, other apoptosis molecules, such as DNA damage-related protein p53, were induced in addition to CHOP protein (Oyadomari *et al.* 2001). In addition, in $CHOP^{-/-}$ mice, pancreatic b-cells were more resistant to nitric oxide-induced apoptosis than those from wild-type mice (Oyadomari *et al.* 2001). Targeted disruption of the CHOP gene could delay b-cell apoptosis and diabetes mellitus in insulin 2 mutation diabetes mice (Oyadomari *et al.* 2002a). Furthermore, $CHOP^{-/-}$ mice were more resistant to neuronal cell death in brain ischaemia (Tajiri *et al.* 2004). However, unlike $CHOP^{-/-}$ mice, pancreatic islets derived from $CHOP^{+/-}$ mice were not resistant to nitric oxide-induced apoptosis (Oyadomari *et al.* 2001), and $CHOP^{+/-}$ mice could not block or delay the development of diabetes caused by insulin mutation (Oyadomari *et al.* 2002a).

In conclusion, our results indicated that intravitreous NMDA injection induced CHOP expression and led to apoptosis in the GCL. Disruption of the CHOP gene gave resistance to NMDA-induced retinal damage. We propose that the ER stress–CHOP pathway is a potential target that may prevent retinal neuronal cell apoptosis induced by excitatory amino acids.

Acknowledgements

We thank Shizuo Akira (Osaka University) for providing the $CHOP^{-/-}$ mice. This work was supported in part by a Grant-in-Aid for Scientific Research from the Ministry of Education, Science, Sports and Culture, Japan and from the Ministry of Health and Welfare, Japan. Commercial relationship policy: N.

References

Alberts B., Johnson A., Lewis J., Raff M., Roberts K. and Walter P. (2002) The endoplasmic reticulum, in *Molecular Biology of the Cell*, 4th edn. pp. 689–709. Garland Science, New York.

Barone M. V., Crozat A., Tabaee A., Philipson L. and Ron D. (1994) CHOP(GADD153) and its oncogenic variant, TLS-CHOP, have opposing effects on the induction of G1/S arrest. *Genes Dev.* **8**, 453–464.

Chaudhary P., Ahmed F. and Sharma S. C. (1998) MK801-a neuroprotectant in rat hypertensive eyes. *Brain Res.* **792**, 154–158.

Chen G., Bower K. A., Ma C., Fang S., Thiele C. J. and Luo J. (2004) Glycogen synthase kinase 3 (GSK3b) mediates 6-hydroxydopamine-induced neuronal death. *FASEB J.* **18**, 1162–1164.

DeGracia D. J. and Montie H. L. (2004) Cerebral ischemia and the unfolded protein response. *J. Neurochem.* **91**, 1–8.

Dkhissi O., Chanut E., Wasowicz M., Savoldelli M., Nguyen-Legros J., Minvielle F. and Versaux-Botteri C. (1999) Retinal TUNEL-positive cells and high glutamate levels in vitreous humor of mutant quail with a glaucoma-like disorder. *Invest. Ophthalmol. Vis. Sci.* **40**, 990–995.

Farrar G. J., Kenna P. F. and Humphries P. (2002) On the genetics of retinitis pigmentosa and on mutation-independent approaches to therapeutic intervention. *EMBO J.* **21**, 857–864.

Gotoh T., Oyadomari S., Mori K. and Mori M. (2002) Nitric oxide-induced apoptosis in RAW 264.7 macrophages is mediated by endoplasmic reticulum stress pathway involving ATF6 and CHOP. *J. Biol. Chem.* **277**, 12 343–12 350.

Gotoh T., Terada K., Oyadomari S. and Mori M. (2004) Hsp70-DnaJ chaperone pair prevents nitric oxide- and CHOP-induced apoptosis by inhibiting translocation of Bax to mitochondria. *Cell Death Differ.* **11**, 390–402.

Hajnoczky G., Davies E. and Madesh M. (2003) Calcium signaling and apoptosis. *Biochem. Biophys. Res. Commun.* **304**, 445–454.

Imai Y., Soda M. and Takahashi R. (2000) Parkin suppresses unfolded protein stress-induced cell death through its E3 ubiquitin-protein ligase activity. *J. Biol. Chem.* **275**, 35 661–35 664.

Inomata Y., Hirata A., Yonemura N., Koga T., Kido N. and Tanihara H. (2003a) Neuroprotective effects of interleukin-6 on NMDA-induced rat retinal damage. *Biochem. Biophys. Res. Commun.* **302**, 226–232.

Inomata Y., Hirata A., Koga T., Kimura A., Singh D. P., Shinohara T. and Tanihara H. (2003b) Lens epithelium-derived growth factor: neuroprotection on rat retinal damage induced by *N*-methyl-D-aspartate. *Brain Res.* **991**, 163–170.

Joo C. K., Choi J. S., Ko H. W., Park K. Y., Sohn S., Chun M. H., Oh Y. J. and Gwag B. J. (1999) Necrosis and apoptosis after retinal ischemia: involvement of NMDA-mediated excitotoxicity and p53. *Invest. Ophthalmol. Vis. Sci.* **40**, 713–720.

Katayama T., Imaizumi K., Manabe T., Hitomi J., Kudo T. and Tohyama M. (2004) Induction of neuronal death by ER stress in Alzheimer's disease. *J. Chem. Neuroanat.* **28**, 67–78.

Kaufman R. J., Scheuner D., Schroder M., Shen X., Lee K., Liu C. Y. and Arnold S. M. (2002) The unfolded protein response in nutrient sensing and differentiation. *Nat. Rev. Mol. Cell Biol.* **3**, 411–421.

Kawahara K., Oyadomari S., Gotoh T., Kohsaka S., Nakayama H. and Mori M. (2001) Induction of CHOP and apoptosis by nitric oxide in p53-deficient microglial cells. *FEBS Lett.* **506**, 135–139.

Kerrigan L. A., Zack D. J., Quigley H. A., Smith S. D. and Pease M. E. (1997) TUNEL-positive ganglion cells in human primary open-angle glaucoma. *Arch. Ophthalmol.* **115**, 1031–1035.

Kitano H., Nishimura H., Tachibana H., Yoshikawa H. and Matsuyama T. (2004) ORP150 ameliorates ischemia/reperfusion injury from middle cerebral artery occlusion in mouse brain. *Brain Res.* **1015**, 122–128.

Kouroku Y., Fujita E., Jimbo A. *et al.* (2002) Polyglutamine aggregates stimulate ER stress signals and caspase-12 activation. *Hum. Mol. Genet.* **11**, 1505–1515.

Kuroiwa S., Katai N., Shibuki H., Kurokawa T., Umihira J., Nikaido T., Kametani K. and Yoshimura N. (1998) Expression of cell cycle-related genes in dying cells in retinal ischemic injury. *Invest. Ophthalmol. Vis. Sci.* **39**, 610–617.

Laabich A., Li G. and Cooper N. G. (2001) Characterization of apoptosis-genes associated with. NMDA mediated cell death in the adult rat retina. *Brain Res. Mol. Brain Res.* **91**, 34–42.

Lam T. T., Abler A. S., Kwong J. M. and Tso M. O. (1999a) *N*-methyl-D-aspartate (NMDA)-induced apoptosis in rat retina. *Invest. Ophthalmol. Vis. Sci.* **40**, 2391–2397.

Lam T. T., Abler A. S. and Tso M. O. (1999b) Apoptosis and caspases after ischemia-reperfusion injury in rat retina. *Invest. Ophthalmol. Vis. Sci.* **40**, 967–975.

Matsumoto M., Minami M., Takeda K., Sakao Y. and Akira S. (1996) Ectopic expression of CHOP (GADD153) induces apoptosis in M1 myeloblastic leukemia cells. *FEBS Lett.* **395**, 143–147.

Mattson M. P. and Chan S. L. (2003) Neuronal and glial calcium signaling in Alzheimer's disease. *Cell Calcium* **34**, 385–397.

McCullough K. D., Martindale J. L., Klotz L. O., Aw T. Y. and Holbrook N. J. (2001) Gadd 153 sensitizes cells to endoplasmic reticulum stress by down-regulating Bcl2 and perturbing the cellular redox state. *Mol. Cell Biol.* **21**, 1249–1259.

Nakagawa T., Zhu H., Morishima N., Li E., Xu J., Yankner B. A. and Yuan J. (2000) Caspase-12 mediates endoplasmic-reticulum-specific apoptosis and cytotoxicity by amyloid-β. *Nature* **403**, 98–103.

Nishitoh H., Matsuzawa A., Tobiume K., Saegusa K., Takeda K., Inoue K., Hori S., Kakizuka A. and Ichijo H. (2002) ASK1 is essential for endoplasmic reticulum stress-induced neuronal cell death triggered by expanded polyglutamine repeats. *Genes Dev.* **16**, 1345–1355.

Oyadomari S. and Mori M. (2004) Roles of CHOP/GADD153 in endoplasmic reticulum stress. *Cell Death Differ.* **11**, 381–389.

Oyadomari S., Takeda K., Takiguchi M., Gotoh T., Matsumoto M., Wada I., Akira S., Araki E. and and. Mori M. (2001) Nitric oxide-induced apoptosis in pancreatic β cells is mediated by the endoplasmic reticulum stress pathway. *Proc. Natl Acad. Sci. USA* **98**, 10 845–10 850.

Oyadomari S., Koizumi A., Takeda K., Gotoh T., Akira S., Araki E. and Mori M. (2002a) Targeted disruption of the Chop gene delays endoplasmic reticulum stress-mediated diabetes. *J. Clin. Invest.* **109**, 525–532.

Oyadomari S., Araki E. and Mori M. (2002b) Endoplasmic reticulum stress-mediated apoptosis in pancreatic b-cells. *Apoptosis* **7**, 335–345.

Paschen W. (2003) Endoplasmic reticulum: a primary target in various acute disorders and degenerative diseases of the brain. *Cell Calcium* **34**, 365–383.

Paschen W. and Frandsen A. (2001) Endoplasmic reticulum dysfunction – a common denominator for cell injury in acute and degenerative diseases of the brain? *J. Neurochem.* **79**, 719–725.

Pereira C., Ferreiro E., Cardoso S. M. and de Oliveira C. R. (2004) Cell degeneration induced by amyloid-b peptides: implications for Alzheimer's disease. *J. Mol. Neurosci.* **23**, 97–104.

Quigley H. A., Nickells R. W., Kerrigan L. A., Pease M. E., Thibault D. J. and Zack D. J. (1995) Retinal ganglion cell death in experimental glaucoma and after axotomy occurs by apoptosis. *Invest. Ophthalmol. Vis. Sci.* **36**, 774–786.

Reme C. E., Grimm C., Hafezi F., Marti A. and Wenzel A. (1998) Apoptotic cell death in retinal degenerations. *Prog. Retin. Eye Res.* **17**, 443–464.

Ron D. and Habener J. F. (1992) CHOP, a novel developmentally regulated nuclear protein that dimerizes with transcription factors C/EBP and LAP and functions as a dominant-negative inhibitor of gene transcription. *Genes Dev.* **6**, 439–453.

Rosenbaum D. M., Rosenbaum P. S., Gupta H., Singh M., Aggarwal A., Hall D. H., Roth S. and Kessler J. A. (1998) The role of the p53 protein in the selective vulnerability of the inner retina to transient ischemia. *Invest. Ophthalmol. Vis. Sci.* **39**, 2132–2139.

Rosner M., Solberg Y., Turetz J. and Belkin M. (1997) Neuroprotective therapy for argon-laser induced retinal injury. *Exp. Eye Res.* **65**, 485–495.

Roy N. S., Nakano T., Keyoung H. M. *et al.* (2004) Telomerase immortalization of neuronally restricted progenitor cells derived from the human fetal spinal cord. *Nat. Biotechnol.* **22**, 297–305.

Sigelman J. and Ozanics V. (1982) Retina, in *Ocular Anatomy, Embryology, and Teratology* (Jakobiec, F. A., ed.), pp. 478–481. Harper and Row, Philadelphia.

Staller P., Sulitkova J., Lisztwan J., Moch H., Oakeley E. J. and Krek W. (2003) Chemokine receptor CXCR4 downregulated by von Hippel-Lindau tumour suppressor pVHL. *Nature* **425**, 307–311.

Sun Q., Ooi V. E. and Chan S. O. (2001) *N*-methyl-D-aspartate-induced excitotoxicity in adult rat retina is antagonized by single systemic injection of MK-801. *Exp. Brain Res.* **138**, 37–45.

Tajiri S., Oyadomari S., Yano S., Morioka M., Gotoh T., Hamada J. I., Ushio Y. and Mori M. (2004) Ischemia-induced neuronal cell death is mediated by the endoplasmic reticulum stress pathway involving CHOP. *Cell Death Differ.* **11**, 403–415.

Takeda K., Matsuzawa A., Nishitoh H., Tobiume K., Kishida S., Ninomiya-Tsuji J., Matsumoto K. and Ichijo H. (2002) ASK1 is essential for endoplasmic reticulum stress-induced neuronal cell death triggered by expanded polyglutamine repeats. *Genes Dev.* **16**, 1345–1355.

Tobiume K., Matsuzawa A., Takahashi T. *et al.* (2001) ASK1 is required for sustained activations of JNK/p38 MAP kinases and apoptosis. *EMBO Report* **2**, 222–228.

Tokuhiro S., Yamada R., Chang X. *et al.* (2003) An intronic SNP in a RUNX1 binding site of. SLC22A4, encoding an organic cation transporter, is associated with rheumatoid arthritis. *Nat. Genet.* **35**, 341–348.

Tsutsumi S., Gotoh T., Tomisato W. *et al.* (2004) Endoplasmic reticulum stress response is involved in nonsteroidal anti-inflammatory drug-induced apoptosis. *Cell Death Differ.* **11**, 1009–1016.

Wax M. B., Tezel G. and Edward P. D. (1998) Clinical and ocular histopathological findings in a patient with normal-pressure glaucoma. *Arch. Ophthalmol.* **116**, 993–1001.

Zinszner H., Kuroda M., Wang X., Batchvarova N., Lightfoot R. T., Remotti H., Stevens J. L. and Ron D. (1998) CHOP is implicated in programmed cell death in response to impaired function of the endoplasmic reticulum. *Genes Dev.* **12**, 982–995.

rich2/stm-stemc/stm-stemc/stm00106/stm0015d06a | smitherj | S=11 | 12/5/05 | 9:40 | 4/Color Figure(s): 1,4 | Art: SC-050124 | Input-??

STEM CELLS®
Tissue-Specific Stem Cells

AQ: 1

Activation of Canonical Wnt Pathway Promotes Proliferation of Retinal Stem Cells Derived From Adult Mouse Ciliary Margin

TOSHIHIRO INOUE,[a,b] TETSUSHI KAGAWA,[b,c] MIKIKO FUKUSHIMA,[a] TAKESHI SHIMIZU,[b] YUTAKA YOSHINAGA,[b] SHINJI TAKADA,[d] HIDENOBU TANIHARA,[a] TETSUYA TAGA[b]

[a]Department of Ophthalmology and Visual Science, Graduate School of Medical Sciences and [b]Department of Cell Fate Modulation, Institute of Molecular Embryology and Genetics, Kumamoto University Graduate School of Medical Science, Kumamoto, Japan; [c]Division of Active Transport, National Institute for Physiological Sciences, Okazaki, Japan; [d]Center for Integrative Bioscience, Okazaki National Research Institutes, Okazaki, Japan

AQ: 3

ABSTRACT

Fn1

Adult retinal stem cells represent a possible cell source for the treatment of retinal degeneration. However, only a small number of stem cells reside in the ciliary margin. The present study aimed to promote the proliferation of adult retinal stem cells via the Wnt signaling pathway. Ciliary margin cells from 8-week-old mice were dissociated and cultured to allow sphere colony formation. Wnt3a, a glycogen synthase kinase (GSK) 3 inhibitor, fibroblast growth factor (FGF) 2, and a FGF receptor inhibitor were then applied in the culture media. The primary spheres were dissociated to prepare either monolayer or secondary sphere cultures. Wnt3a increased the size of the primary spheres and the number of Ki-67–positive proliferating cells in monolayer culture. The Wnt3a-treated primary sphere cells were capable of self-renewal and gave rise to fourfold the number of secondary spheres compared with nontreated sphere cells. These cells also retained their multilineage potential to express several retinal markers under differentiating culture conditions. The Wnt3a-treated cells showed nuclear accumulation of β-catenin, and a GSK3 inhibitor, SB216763, mimicked the mitogenic activity of Wnt3a. The proliferative effect of SB216763 was attenuated by an FGF receptor inhibitor but was enhanced by FGF2, with Ki-67–positive cells reaching over 70% of the total cells. Wnt3a and SB216763 promoted the proliferation of retinal stem cells, and this was partly dependent on FGF2 signaling. A combination of Wnt and FGF signaling may provide a therapeutic strategy for in vitro expansion or in vivo activation of adult retinal stem cells. STEM CELLS *2006;0:000–000*

INTRODUCTION

The ciliary marginal zone is widely known to contain immature retinal cells that continue to divide throughout life in both amphibians and fish [1–7]. Recently, a limited number of ciliary margin cells in adult rodents were demonstrated to sustain stem cell characteristics in vitro [8, 9]. From a therapeutic viewpoint, stem cells residing in an adult tissue, if able to be expanded in vitro or activated in vivo, have a significant advantage in autologous transplantation or activation of endogenous stem cells because they can overcome immune rejection and the ethical concerns associated with using embryonic or neonatal tissues. Therefore, retinal stem cells in the adult ciliary margin have been highlighted as a possible cell source for stem cell therapies. However, it is debatable whether these cells can provide the copious stem cell pools required for therapy because a single primary sphere colony can only generate six to eight secondary

AQ: 2

Correspondence: ?. Received March 18, 2005; accepted for publication June 28, 2005. ©AlphaMed Press 1066-5099 doi: 10.1634/stemcells.2005-0124

spheres in the presence of fibroblast growth factor (FGF) 2 [9]. In addition, a limited number of primary spheres can be generated from individual adult eyes; only approximately 55 spheres were obtained from individual adult rodent eyes [9], and these spheres showed lower and restricted proliferation potential compared with neural stem cells derived from the adult subventricular zone [10]. Hence, improved and efficient strategies to expand retinal stem cells are required.

Wnt proteins are secreted lipid-modified signaling molecules that regulate cell proliferation and cell fate in various tissues in vertebrate embryos and can activate different intracellular signaling cascades, including the canonical pathway, c-Jun N-terminal kinase pathway, Ca^{2+} pathway, and focal adhesion kinase pathway (reviewed by Pandur et al. [11]). In the canonical pathway, Wnt protein binding to Frizzled (Fzd) and low-density lipoprotein receptor–related proteins (LRP) causes inactivation of glycogen synthase kinase (GSK) 3β and Axin, respectively. The inactivation of these proteins stabilizes β-catenin, which subsequently accumulates in the cell nucleus and activates the transduction of target genes that are crucial in the G1–S-phase transition, such as cyclin D1 or c-Myc (reviewed by Willert et al. [12]). Therefore, the canonical Wnt pathway contributes to cell proliferation in different types of stem cells [13–17].

During eye development in the chick, various components of Wnt signaling are expressed. Kubo et al. [18] demonstrated that Wnt2b can promote the proliferation of chick embryonic ciliary margin cells that can yield differentiated retinal progeny through activation of the canonical pathway. This finding encouraged us to explore whether Wnt signaling could promote the proliferation of adult retinal stem cells from the mammalian ciliary margin. In the present study, we demonstrate that Wnt3a increased the size of the spheres derived from ciliary margin. Wnt3a also increased the number of cells expressing Ki-67 and bromodeoxyuridine (BrdU) incorporation in triturated sphere cell cultures. More importantly, Wnt3a-treated sphere cells retained multipotency and formed a greater number of secondary spheres than nontreated cells, indicating that Wnt signaling functions on self-renewal of retinal stem cells (secondary sphere-forming ability). We further suggest that the Wnt3a-mediated increase in self-renewal involved the canonical pathway. Interestingly, the mitogenic effect of Wnt signaling was enhanced by exogenous FGF2 and attenuated by a FGF receptor inhibitor. Our results provide a basis for the development of useful strategies for the in vitro expansion of adult retinal stem cells.

Materials and Methods

Isolation and Culture

Eight-week-old C57Bl6 mice and green fluorescent protein (GFP) transgenic mice were used to prepare adult retinal stem cells as previously reported [9]. All studies were conducted in accordance with the guidelines of the Kumamoto University Center for Animal Resources and Development. Dissociated cells were cultured at clonal density for 5 days on six-well dishes (Nunc, Naperville, IL, http://www.nuncbrand.com) precoated with poly-HEME (Sigma-Aldrich, St. Louis, http://www.sigmaaldrich.com) in Dulbecco's modified Eagle's medium/F-12 medium (Invitrogen, Carlsbad, CA, http://www.invitrogen.com) containing B27 (Invitrogen) and various supplements: FGF2 (recombinant human FGF2; R&D Systems, Minneapolis, http://www.rndsystems.com), Wnt3a (recombinant mouse Wnt3a; catalog no. 1324-WN; R&D Systems), or SB216763 (Biomol Research Laboratories, Plymouth Meeting, PA, http://www.biomol.com). The cells were then triturated with enzymatic solution [9], replated on chamber slides (Nunc) precoated with poly-L-ornithine (Sigma-Aldrich) and fibronectin (Life Technologies, Gaithersburg, MD), and cultured for 2 days in B27/DMEM/F-12 containing various supplements: FGF2, Wnt3a, SB216763, Fzd-8-CRD (recombinant mouse Fzd-8/Fc chimera; R&D Systems), or SU5402 (EMD biosciences, San Diego, http://splash.emdbiosciences.com). The S-phase cells in these culture condition were further monitored by BrdU incorporation. After 2-day cultures with or without Wnt3a, the cells were pulse labeled with 10 μM BrdU for 4 hours, incubated in BrdU-free media for an additional 2 hours, and fixed for the immunochemical analyses. For secondary sphere formation, B27/DMEM/F-12 containing FGF2 and epidermal growth factor (EGF) (recombinant human EGF; R&D Systems) was used. To promote retinal cell differentiation, triturated cells were cultured for 7 days as previously described [9]. All cultures were maintained at 37°C in 5% CO_2.

Reverse Transcription–Polymerase Chain Reaction

Total RNA was isolated from sphere cells using Trizol (Invitrogen). Reverse transcription was performed on 2 μg of RNA using Superscript II (Invitrogen) according to the manufacturer's protocol. Reverse transcription products were amplified by polymerase chain reaction (PCR) using KOD-plus (Toyobo, Osaka, Japan, http://www.toyobo.co.jp) and gene-specific primers [19–22] under standard reaction conditions with an initial 2-minute denaturation step followed by 24 to 30 cycles of 94°C for 15 seconds, 58°C for 30 seconds, and 68°C for 60 seconds.

Immunocytochemistry

The cells were fixed with 4% paraformaldehyde for 10 minutes and then blocked with 3% goat serum in phosphate-buffered saline containing 0.1% Triton X-100 for 30 minutes. The cells were incubated for 2 hours with one or two of the following specific primary antibodies at the stated dilutions: mouse monoclonal anti–Ki-67 (1:200; BD Biosciences, Franklin Lakes, NJ,

http://www.bdbiosciences.com) as a cell-division marker; rat monoclonal anti-BrdU (1:40; Abcam, Cambridge, UK, http://www.abcam.com) as an S-phase cell marker; rabbit antiactive caspase-3 (1:200; BD Biosciences) as a cell-death marker; mouse monoclonal antirhodopsin (1:200; Chemicon International, Temecula, CA, http://www.chemicon.com/) as a rod photoreceptor cell marker; mouse monoclonal antisyntaxin (1:200; Sigma-Aldrich) and rabbit polyclonal anti-Pax6 (1:500; Chemicon International) as amacrine cell markers; mouse monoclonal antiglutamine (Gln) synthetase (1:200; Chemicon International) as a Müller glia marker; and mouse monoclonal anti–β-catenin (1:250; BD Biosciences). The cells were examined by epifluorescence after incubation for 30 minutes in Alexa 488- and/or Alexa 596-conjugated secondary antibodies (Molecular Probes, Eugene, OR; http://www.probes.com). Cell nuclei were counterstained with Hoechst 33258 (Nacalai Tesque, Kyoto, Japan, http://www.nacalai.co.jp). Negative controls were performed in parallel during all immunocytologic processing by omission of a primary antibody. No fluorescent labeling was observed in the negative controls. Images were obtained using an AX70 fluorescence microscope (Olympus, Tokyo, http://www.olympus-global.com) or TCS SP2 AOBS confocal microscope (Leica Microsystems, Wetzlar, Germany, http://www.leica-microsystems.com).

Statistical Analysis

The data represent the mean ± standard deviation of three separate experiments. For cytochemical studies, five randomly selected fields per sample were analyzed in each condition. Statistical significance was determined by Student's two-tailed *t*-test.

RESULTS

Stem Cell Properties of Ciliary Margin Cells

To ensure the existence of retinal stem cells from the ciliary margins of 8-week-old mice, the dissociated ciliary margin cells were cultured in the nonadherent condition at a clonal density. After 5 days in culture, sphere formation was observed. To further examine whether these sphere colonies were generated by the proliferation of single cells, ciliary margin cells were prepared from both GFP-expressing and wild-type mice, and the cell mixture was cultured at a clonal density for 5 days according to the method of Tropepe et al. [9]. Separate GFP-positive and GFP-negative spheres were observed (Fig. 1), demonstrating that the colonies were not derived from cell aggregation but instead arose clonally. Green spheres contained some dark dots, which might look like GFP-negative cells. However, they were not actually GFP-negative cells but differentiated pigment epithelial cells whose pigment may mask or impede the green color. These sphere cells were capable of generating secondary

F1

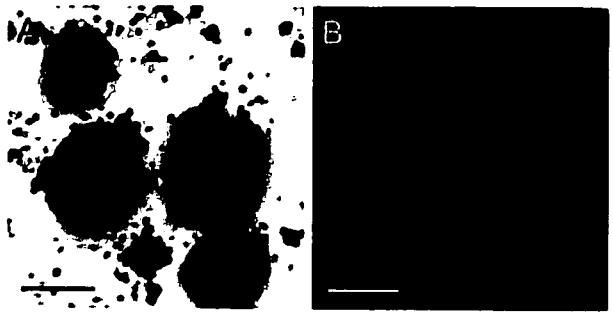

Figure 1. Clonal sphere formation of retinal stem cells from the adult ciliary margin. Phase (**A**) and fluorescence (**B**) photomicrographs are shown. Dissociated adult ciliary margin cells from GFP-expressing and wild-type mice were mixed and cultured in the nonadherent condition for 5 days. The mixture of dissociated cells generated distinctive spheres. Scale bars = 100 μm.

spheres and differentiating to express different retinal cell–specific markers, rhodopsin, syntaxin, and Pax6, under culture conditions that promoted retinal cell differentiation [8] (Table 1). Thus, the sphere cells from the ciliary margin possessed the stem cell characters of self-renewal and multilineage potential.

T1

Effect of Wnt3a on Cell Proliferation

Because a limited number of primary spheres can be generated from individual adult eyes, improved and efficient strategies that expand the retinal stem cell pool by promoting cell proliferation are required. Wnt is a good candidate for this because it acts as a mitogen for immature retinal cells [18]. We first examined the expression of Wnt receptor genes in the sphere cells by reverse transcription–PCR. As shown in Figure 2A, gene products specific for Fzd-1, -3, -4, -6, -7, and -8 were amplified, whereas no signals for Fzd-2, -5, and -9 were detected. LRP-5 and -6, which are known to be indispensable receptors for the canonical Wnt pathway, were expressed. These results suggest that sphere cells from the adult ciliary

F2

Table 1. Sphere cells expanded by Wnt3a or SB216763 retained their multilineage potential

	FGF2	Wnt3a	SB216763
Rhodopsin	10.2 ± 1.8	12.3 ± 2.4	10.6 ± 3.9
Syntaxin/Pax6	4.7 ± 1.2	3.9 ± 1.3	5.1 ± 0.2
Gln Synthetase	24.0 ± 5.6	24.0 ± 10.0	26.3 ± 10.4

The average percentage (± standard deviation) of cell types in the number of nuclei stained with Hoechst is shown in the column. Sphere colonies were grown in fibroblast growth factor 2 (FGF2)-, Wnt3a-, orSB216763-containing medium for 5 days. Thereafter, each sphere colony was plated and cultured for 21 days under conditions that promote retinal cell differentiation. The sphere-derived cells expressed several retinal cell–specific markers, such as rhodopsin as rod photoreceptors, Pax6 and syntaxin as amacrine cells, or Gln synthetase as Müller glia. In respect of these markers, any marked deviation of retinal cell fate was not observed among conditions of sphere formation.

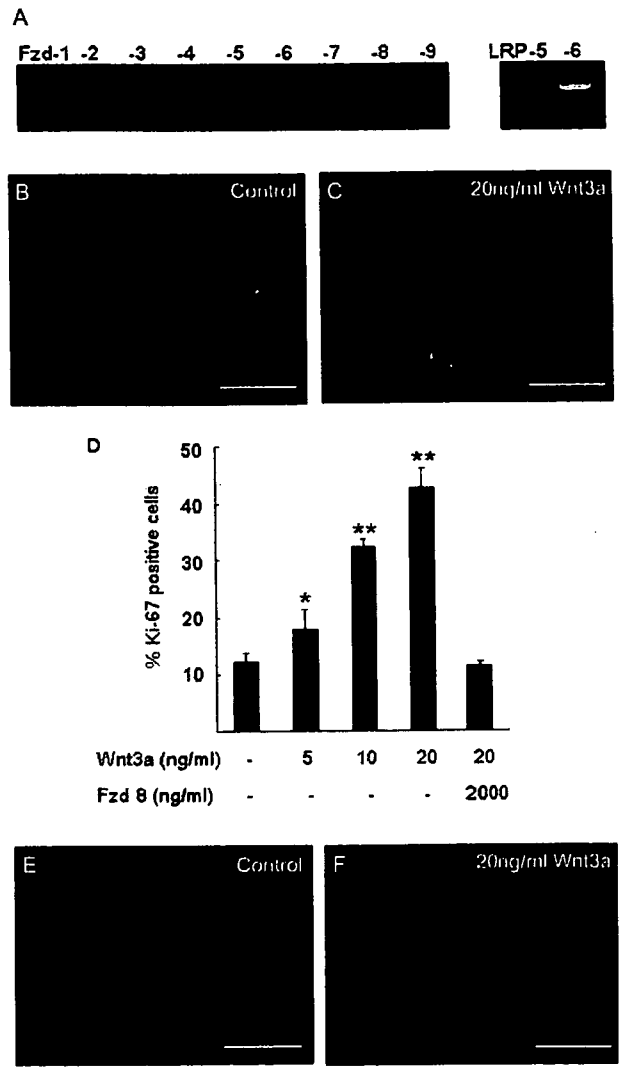

F3 **Figure 2.** Effect of Wnt3a on the cell-division markers. **(A):** Expression of Fzd family and LRP-5/6 mRNAs in the primary sphere cells were examined by reverse transcription–polymerase chain reaction. Gene products specific for Fzd-1, -3, -4, -6, -7, and -8 and LRP-5 and -6 were amplified. **(B–F):** Primary spheres were triturated and cultured in the adherent condition with various concentrations of Wnt3a for 48 hours. In the control cultures, 2.5 μg/ml dimethyl sulfoxide was added to the medium. The fluorescence photomicrographs **(B, C)** show merged images of Hoechst (blue) and anti–Ki-67 antibody (green) labeling. The number of Ki-67–positive cells in the culture containing 20 ng/ml Wnt3a **(C)** is greater than that in the control culture **(B)**. Quantification of Ki-67–positive cells **(D)** shows that Ki-67–positive cells increase in a Wnt3a dose-dependent manner, and Fzd-8-CRD (a Wnt antagonist) blocks this effect. All data represent the means ± standard deviations of three separate experiments. The fluorescence photomicrographs **(E, F)** show merged images of Hoechst (blue) and anti-bromodeoxyuridine (BrdU) antibody (red). In the presence of Wnt3a, the number of BrdU-incorporating cells is greater than that in the control condition. Scale bars = 100 μm. $*p < .05$, $**p < .01$ compared with control cultures.

margin have the prerequisites to react in response to Wnt proteins. To address the effect of Wnt signaling on the proliferation of adult retinal stem cells, the spheres were dissociated and cultured in the adherent condition for 48 hours in the presence of recombinant Wnt3a at a series of graded concentrations. The proliferative response was assayed by immunocytochemical staining for Ki-67, a cell-division marker [23]. Ki-67-positive cells were increased in a dose-dependent manner after the addition of Wnt3a (Figs. 2B–2D). This effect was maximal at 20 ng/ml Wnt3a, when the Ki-67-positive cells increased by 3.5-fold compared with control cultures. Since the recombinant Wnt3a used was only refined to 75% purity according to the manufacturer's description, there was a possibility that some of the impurities could have influenced the cell proliferation. Thus, Fzd-8-CRD, a Wnt antagonist [24, 25], was applied to the dissociation culture together with the recombinant Wnt3a. Sufficient dose of Fzd-8-CRD decreased the number of Ki-67–positive cells to the basal level (Fig. 2D), confirming the mitogenic effect of Wnt3a on sphere-derived cells. To examine DNA synthesis in the sphere-derived cells, they were pulse-labeled with BrdU for 4 hours. In the presence of 20 ng/ml Wnt3a, the number of BrdU-positive cells was increased from 10.2% ± 2.5% to 18.8% ± 1.6% ($p < .01$) (Figs. 2E, 2F), consistent with the increase in Ki-67–positive cells. Under all of the above conditions, there was no difference in the cell death estimated by immunocytochemical detection of activated caspase-3 (data not shown).

To further estimate the proliferative response, we assessed the size of the primary spheres (50 μm or more of the diameter) with or without Wnt3a. After a 5-day culture in vitro, the diameter of the spheres was increased in the presence of 20 ng/ml Wnt3a (Fig. 3A), consistent with the data in the adherent condition described above. Notably, the average volume of the Wnt3a-treated spheres was threefold larger than that of the control spheres, although various sizes of spheres appeared in Wnt3a-containing cultures. To exclude the possibility that Wnt3a increased each cell volume, the nuclei of sphere cells were stained by Hoechst 33258 and the cell densities were examined by the confocal microscope. The cell densities of the Wnt3a-treated spheres were nearly equal to those of control spheres (Figs. 3B, 3C), confirming that the size of the spheres was reflected in the cell number but not the cell size. On the contrary, there was no significant difference between the number of primary sphere colonies in the Wnt3a-containing and control cultures (data not shown), suggesting that Wnt3a did not affect the number of cells capable of forming primary spheres nor transform nonsphere forming cells into sphere-forming stem cells. Taken together, Wnt3a promotes the proliferation of sphere-forming cells from the adult ciliary margin.

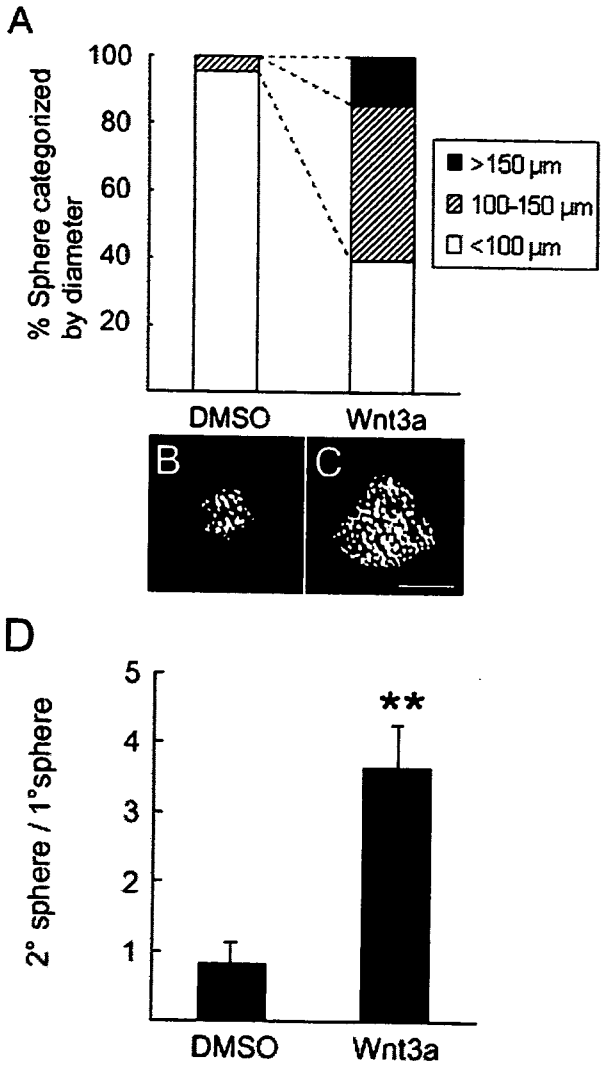

Figure 3. Effect of Wnt3a on the sphere formation. **(A):** Percentages of spheres categorized by their diameter. Isolated ciliary margin cells were plated at 20,000 cells/ml and cultured in the nonadherent condition with 20 ng/ml Wnt3a for 5 days, and the sphere size was estimated. In the control cultures, 2.5 μg/ml dimethyl sulfoxide (DMSO) was added to the medium. A large proportion of spheres in the Wnt3a-containing culture are greater than 100 μm in diameter, whereas most of the spheres in the DMSO-treated control culture have diameters of 100 μm or less. The results are representative of three independent experiments. The percentages of sphere-forming cells with DMSO and Wnt3a were 0.098% ± 0.02% and 0.12% ± 0.03%, respectively. **(B, C):** Confocal microscopic images of the nuclei-counterstained primary spheres. The cell densities of the Wnt3a-induced large-sized spheres **(C)** were nearly equal to that of small-sized spheres in the control condition **(B)**. **(D):** Numbers of secondary spheres generated from primary spheres. Primary spheres were triturated and cultured in the nonadherent condition for 7 days in the presence of fibroblast growth factor 2 and epidermal growth factor. The number of secondary spheres generated from Wnt3a-treated spheres is greater than that from DMSO-treated control spheres. The results are the means ± standard deviations of three replicates. Scale bar = 100 μm. $^{**}p < .01$ compared with control cultures.

Characterization of Cells Expanded by Wnt3a

Although Wnt3a promoted the proliferation of sphere cells, it remained unclear whether this proliferation was accompanied by self-renewal of the adult retinal stem cells. If Wnt3a promoted self-renewal, the Wnt3a-treated cells should retain their stem cell characters even after proliferation. To test this hypothesis, individual primary sphere colonies cultured in the presence or absence of Wnt3a were dissociated and allowed to form secondary spheres. The Wnt3a-treated cells generated fourfold the number of secondary sphere colonies compared with dimethylsulfoxide (DMSO)-treated cells from a single primary sphere (Fig. 3D). In parallel with the increased sphere size after Wnt3a treatment, the Wnt3a-treated spheres contained greater numbers of stem cells than the control DMSO-treated spheres, indicating that Wnt 3a promotes proliferation of sphere-derived cells, including retinal stem cells.

To further characterize the cells expanded by Wnt3a, we next examined the multilineage potential of Wnt3a-treated cells. Sphere colonies grown in Wnt3a-containing medium were dissociated and cultured for 7 days under conditions that promote retinal cell differentiation as described above. The Wnt3a-treated cells expressed several retinal cell–specific markers, such as rhodopsin as rod photoreceptors (Fig. 4A), Pax6 and syntaxin as amacrine cells (Fig. 4B), or Gln synthetase as Müller glia (Fig. 4C). In respect of these markers, Wnt3a-treated cells did not show any marked deviation of retinal cell fate compared with FGF2-treated cells (Table 1). Thus, sphere cells expanded by Wnt3a retained their multilineage potential.

Activation of the Canonical Wnt Pathway

To investigate whether Wnt3a protein activates the canonical Wnt pathway in sphere-derived cells from the adult ciliary margin, we next examined the subcellular localization of β-catenin by immunocytochemistry. β-catenin is a coactivator of LEF/TCF-dependent transcription but is normally phosphorylated by GSK3β and quickly degraded. Activation of the canonical Wnt pathway inhibits the kinase activity of GSK3β, resulting in relocation of stabilized β-catenin to the nucleus. After trituration of primary spheres derived from the adult ciliary margin, the cells were cultured in the adhesive condition for 1 day and then treated with or without 20 ng/ml Wnt3a for 2 hours. The Wnt3a-treated cells showed nuclear accumulation of β-catenin (Fig. 5B, Wnt3a). In contrast, a low level of β-catenin was observed under the plasma membrane and in the cytoplasmic region of nontreated cells (Fig. 5A, control). Thus, Wnt3a is capable of activating the canonical Wnt pathway in sphere-derived cells.

Effect of a GSK3 Inhibitor on Proliferation

Despite the activation of the canonical pathway by Wnt3a, it remained unclear whether its activation was involved in pro-

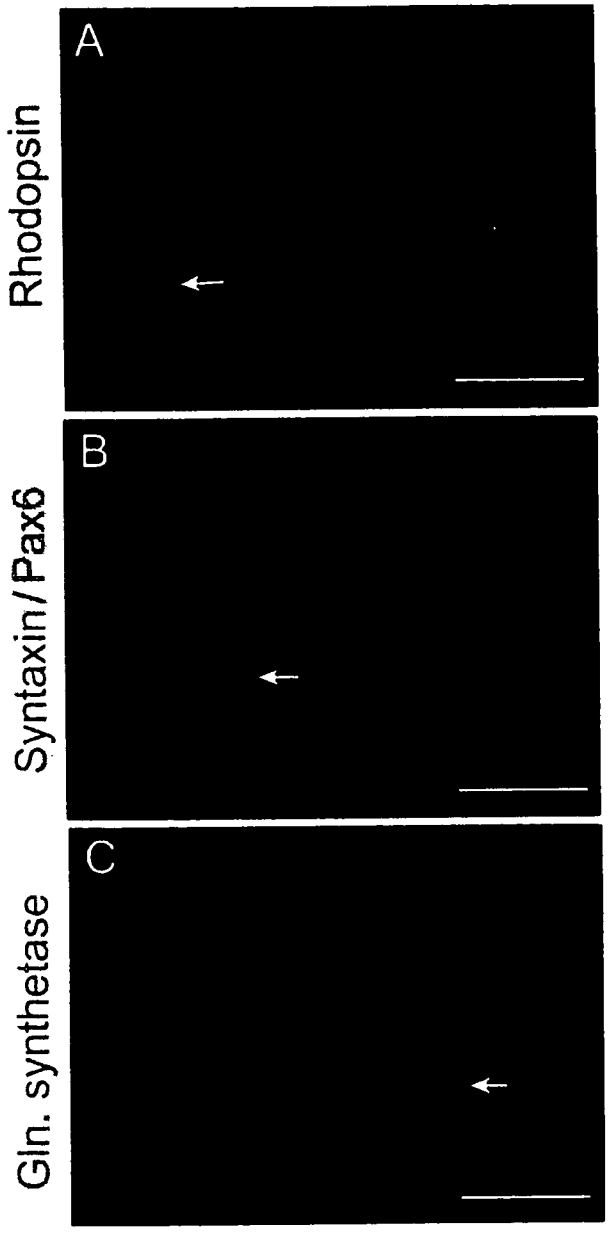

Figure 4. Fluorescence photomicrographs of differentiated cells. Wnt3a-treated sphere cells were triturated and cultured under conditions that promote retinal cell differentiation for 7 days. The Wnt3a-treated cells expressed several retinal cell–specific markers, such as rhodopsin as rod photoreceptors (**A**), Pax6 and syntaxin as amacrine cells (**B**), or glutamine (gln) synthetase as Müller glia (**C**). Scale bars = 100 μm.

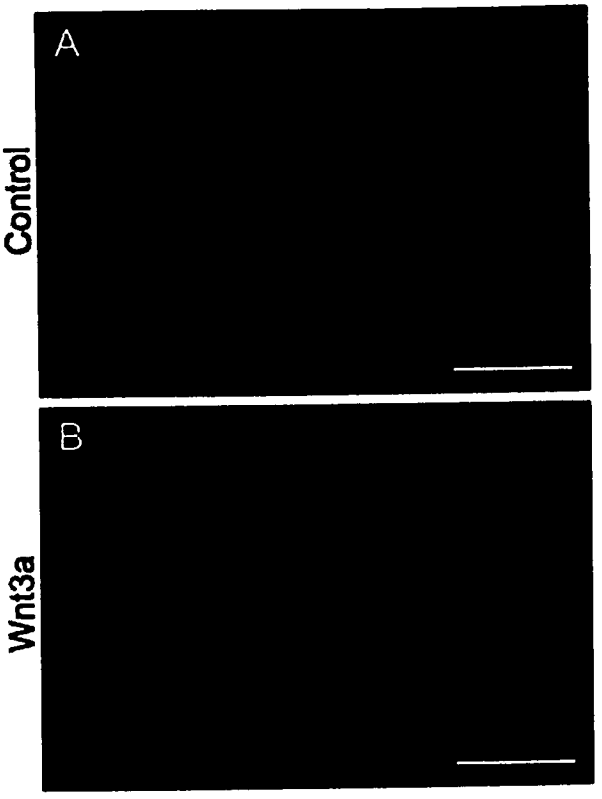

Figure 5. Nuclear translocation of β-catenin in the sphere-derived cells induced by Wnt3a. The localization of β-catenin was examined by immunohistochemistry at 2 hours after the addition of 2.5 μg/ml DMSO (**A**) or 20 ng/ml Wnt3a (**B**). (**A**): β-catenin is observed in the cytoplasm and plasma membrane. (**B**): Wnt3a-treated cells show nuclear accumulation of β-catenin. Scale bars = 100 μm.

moting the proliferation of sphere-derived cells. Thus, we investigated the effect of SB216763, a specific GSK3 inhibitor [26]. GSK3β is a key enzyme in the canonical Wnt pathway that destabilizes β-catenin, and thus SB216763 addition is supposed to mimic Wnt3a stimulation [17, 27]. SB216763 treatment of sphere-derived cell cultures increased Ki-67–positive cells in a dose-dependent manner (Fig. 6A). This effect was maximal at 2.5 μM, when the number of Ki-67–positive cells increased by twofold compared with control cultures. Moreover, the sphere size was increased by SB216763 addition (Fig. 6B). Thus, the GSK3 inhibitor alone mimicked the Wnt3a activity on the proliferation of sphere-derived cells, suggesting that activation of the canonical Wnt pathway was involved in the enhancement of proliferation of sphere-derived cells. Moreover, the SB216763-treated cells expressed several retinal cell–specific markers under conditions that promote retinal cell differentiation and did not show any marked deviation of retinal cell fate compared with FGF2-treated cells (Table 1). Thus, sphere cells expanded by SB216763 retained their multilineage potential.

F6

Cooperative Effect of FGF and Wnt Signaling

Adult retinal stem cells from the ciliary margin have been reported to release a small amount of endogenous FGF2 that promotes sphere formation since antibodies to FGF2 caused a reduction in the number of spheres [9]. To explore the effect of FGF2 on the canonical Wnt pathway, we used SU5402, a small